3-21-2013

Modeling Sodium Iodide Detector Response Using a Parametric Equations

Neeraj Sethi

Follow this and additional works at: https://scholar.afit.edu/etd

Part of the Nuclear Commons

MODELING SODIUM IODIDE DETECTOR RESPONSE USING PARAMETRIC EQUATIONS

THESIS

Neeraj Sethi, Major, USA

AFIT-ENP-13-M-30

DEPARTMENT OF THE AIR FORCE
AIR UNIVERSITY

AIR FORCE INSTITUTE OF TECHNOLOGY

Wright-Patterson Air Force Base, Ohio

AFIT-ENP-13-M-30

Modeling Sodium Iodide Detector Response Using Parametric Equations

THESIS

Presented to the Faculty

Department of Engineering Physics

Graduate School of Engineering and Management

Air Force Institute of Technology

Air University

Air Education and Training Command

In Partial Fulfillment of the Requirements for the

Degree of Master of Science in Nuclear Engineering

Neeraj Sethi, BS

Major, USA

March 2013

DISTRIBUTION STATEMENT A.

APPROVED FOR PUBLIC RELEASE; DISTRIBUTION UNLIMITED

Modeling Sodium Iodide Detector Response Using Parametric Equations
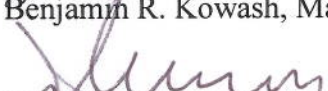
Neeraj Sethi, BS
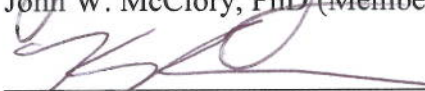
Major, USA

Approved:

Benjamin R. Kowash, Maj, USAF (Chairman)

13 Mar 2013
Date

John W. McClory, PhD (Member)

13 Mar 2013
Date

Kevin C. Gross, PhD (Member)

13 Mar-2013
Date

Abstract

This research demonstrated that parametric equations based on detector response generated by detailed Monte Carlo simulation models can be used to quickly produce expected detector response without running lengthy Monte Carlo simulations. This research utilizes the relationship between source location, background radiation and detector placement to quantify an expected detector response from a 3x3 sodium iodide gamma detector. A parametric equation is developed to calculate the detector response as a function of distance and source photon energy. Using Monte Carlo N-Particle Transport Code MCNP particle current and pulse height tally functions, backscattering photons are quantified as a function of material thickness and energy distribution. It is discovered that changes in the Compton region of the detector spectrum are most apparent in the 100 keV – 350 keV energy range and the threshold thicknesses for generating maximum backscatter from concrete occurs at 16 cm and at 3 cm from steel. Next, configurations of three source – detector – scattering medium arrangements were modeled in MCNP using the pulse height tally functions, integrated over a 70 keV – 360 keV energy window and plotted as a function of the detector distance from the scattering medium. Once fitted, the resulting fit equations described the effects on detector response from the backscattered photons from any wall in a box shaped space. The superposition of the individual scattering contributions from six surfaces made up the total scattering contribution and predicted the overall expected detector response. The same data sets were also plotted and fitted as a function of distance and energy to produce 3 dimensional parametric equations that predicted detector response over various distances and gamma energies. In order to compare the

calculated responses to the experimental results the simulation geometry was re-created in an experiment using a 662 keV Cs-137 source in a room with concrete walls. The normalized superposition and 3D superposition calculated responses were within 4% of the observed responses.

Acknowledgements

I would like to thank Maj Kowash and Dr. Justin Clinton for their help and guidance.

<div align="right">Neeraj Sethi</div>

Table of Contents

List of Figures

List of Tables

I.   Introduction

1.1   Relevance of work

Often when faced with the task of locating an unknown gamma source in a complex environment, the first step is to simulate the proposed detection problem in a modeling program. It is difficult to accurately model the gamma transport because of source photon scattering from the surrounding materials and attenuation. Radiation transport tools like Monte Carlo N-Particle Code (MCNP) can model and simulate the radiation flux created by a source using geometrically accurate models of the complex environment, but increasing the complexity of a simulation can increase the corresponding computational time. In a scenario where quick source identification is required a faster method of predicting detector response is needed. Accurately modeling detector response in urban areas that include widely differing materials presents an additional challenge, as even the building materials can contribute to elevated background levels. K-40 activity can range up to 4000 Bq/kg in natural stone and there is up to 2200 Bq/kg of Ra-226 activity in bricks [1]. Radiation measurements on granite surfaces can show levels similar to those from low-grade uranium mine tailings [1]. These levels raise the background and create additional challenges in extracting relevant data from spectrum of low energy sources.

DTRA has funded a proposed methodology that uses Polarimetric-Hyperspectral Imagery (PHSI) to characterize the environment so that background radiation can be predicted. Characterization of the environment could be used to optimize emplacement of existing detection systems. However, before this can occur, one must understand the photon particle flux in a given space as well as the effects of geometry and material composition to the detection problem. This research focuses on developing techniques and identifying (physical) parameters that affect

1

the gamma flux in a given space. Simulations of a simple box shaped space and experimental

spaces were modeled in MCNP software and the resulting data was analyzed to assess the effects

of varying types of materials and geometry on the detector responses. It was assumed that the

modeled detector response was a direct reflection of the flux in a space. At the same time

physical experiments were conducted with the same geometry as the simulation to verify the

results from the simulations. Once the models were verified and the resulting data analyzed,

parametric equations were developed that calculated the expected response in a simple box

shaped space. This research serves as a first step that demonstrates that detector response can be

calculated without using modeling software.

1.2   Hypothesis

Fast gamma radioisotope identification is possible without using computationally

intensive MCNP models. There is a relationship between source location, activity, nuclear

character, background radiation and optimized detector placement that can be quantified using

parametric equations. This research develops this relationship using MCNP models,

experimentally obtained gamma ray spectra, and a methodology that will maximize the detection

likelihood in a complex scene.

II.   Background

2.1   Detection

The principal purpose of this project is to determine the presence of a gamma radiation source during short collection time windows and to infer material identities from the Compton region of the gamma spectrum. In a scenario where source identification is required quickly, a detector is more likely to register changes in Compton spectra rather than the peaks region of the spectrum. The gamma interactions with the surrounding materials far outnumber the direct photon interaction with the detector. A fraction of these scattered photons register in the detector and become apparent in the Compton region of a spectrum. Current detection approaches improve peak signals by reducing the background by shielding against it; obviously the simplest way to improve the sensitivity of a gamma spectrometer is to reduce the background counts. However, this is not always possible as equipment specifically designed to conduct the Compton-suppression gamma-spectrometry are bulky and require considerable logistical support to operate and therefore are not practical for field use. Additionally, in a scenario where the source is shielded, only Compton spectra may be visible to the detector. A novel approach is needed to utilize available detectors to identify sources using information in the Compton region.

2.1.1   Current Detection Methodologies

In 2001 a group of woodcutters in Lja, Georgia found two 'objects' in the forest (unshielded strontium-90 sources, each approx. 30,000 Ci). The sources were located under a rock, on the edge of a 50m-deep 30°slope [1]. Current detection methodologies use count rate above the background to establish the presence of a source and peak counts above background to establish source identity; a human is potentially put at risk in collecting the spectrum until good

resolution is achieved. However, given a 30,000 Ci source surrounded by ample scattering medium, it would be far safer to collect spectra with a greater standoff. Had the same scenario occurred under threat of physical harm, collecting data expeditiously without exposing the collection team is even more critical to the data collector's safety. However, with greater standoff the peak energy photon interactions in a detector decrease and the Compton scattering increases. A method that exploits the Compton region instead of resolving the peak for identifying radioactive sources would potentially be quicker and safer.

2.1.2 Proposed Methodology

Consider the following example: A vehicle containing U-235 travelling east to west in an urban environment travels at 15 miles per hour. A fixed location NaI detector may only see the vehicle for 2 – 5 seconds before the photons from the source disappear. Typical urban traffic lights are set for 30 seconds stop time so the longest the photons may interact with the detector is increased to up to 40 seconds. Such low count times coupled with low radioactivity of SNM make for a difficult detection problem. MCNP can predict the response even for low count models however creating models for a variety of geometries with low error predictions take valuable time. A well developed parametric equation can shorten the time to predict the detector response without running MCNP.

A library containing the source interaction with scattering materials and the detector response (in varying geometrical configuration) can be created using MCNP or similar software packages. Once the data is gathered the analysis should result in a multi parameter equation that can be used to predict detector response for a given configuration. This research studies a source and detector in a constant geometry and varies the distance from a wall that acts as a scattering medium. In reality the source, scattering medium and geometry can change position, energy

4

value and orientation. Any time one of these variables changes, the detector response changes as well. A parametric equation is needed to describe the relationship between source energy, geometry and detector response. Using this equation a detector response can be calculated for varying geometries and source strength without running lengthy simulations. An attempt at developing a methodology to provide such an equation is explored in this research.

III. Theory

3.1 Scattering

Scattered photons register in the Compton continuum of a spectrum. The differences in the Compton continuum of various materials can be used to create a library of signatures for sources in similar geometry and attenuation configurations.

Scattering is a well known phenomenon used in non-destructive testing studies to quantify defects in target materials. It is known that the energy of backscattered photons is a function of backscatter angle. Typical scattering studies use a collimated source to form a beam at an incident angle upon a target material. This research uses isotropically emitting sources which increases the range of incident photon angle upon the target material. In both cases the scattering phenomenon is angle and energy dependent and is described by the Compton scattering equation, where $E_{\gamma'}$ and E_{γ} are the scattered and the incident energies.

$$E_{\gamma'} = \frac{E_{\gamma}}{1 + \frac{E_{\gamma}}{m_e c^2}(1 - \cos\theta)} \tag{3.1}$$

Scattering is material dependent and the number of backscattered photons increases according to the target thickness until some threshold thickness is reached. Once scattered, photons are distributed over a range of energies. A comparison of the backscatter energy distribution as a function of angle is presented in Table 1 where modeled backscatter energy is compared to experimental energy values as the backscattering angle is changed for a 662 keV beam source [2]   .

6

Table 1 Comparison of a single scattering peak with a simulated and experimental geometry backscattered angle ranging from 60 to 120 degrees [9]. The energy of the backscatter photons varies with the angle at which the photon was backscattered.

Back-scattered angle	Theoretical (keV)	Simulation (keV)	Experiment (keV)
60	401.61	396	395.51
70	357.26	351	352.43
80	319.63	310	317.24
90	288.31	287	287.14
100	262.59	256	259.01
110	241.68	236	241.72
120	224.88	222	227.52

The target and the source are kept at a constant angle but as the detector moves it registers different energy values at different angles. This means that that the backscattered photons contain information that can be utilized for inferring source and scattering medium geometry as well as information about the source energy that could be used for identifying the energy of the potential source.

The potential photon gain from scattering and the energy characteristics of the backscattered photons can be modeled in MCNP using the surface current (F1) and pulse height (F8) tallies. In the F1 tally mode, the reverse photon current should be higher closest to the scattering wall than at farther distances. Similarly, in the F8 tally mode, the net count should be higher in the Compton region at distances closest to the scattering wall than at farther distances.

3.2 Spectral Features

3.2.1   Peak Region

Spectral peaks are the most obvious way of identifying a gamma-emitting radioactive

source. In case of a mono-energetic photon source, the peak represents the pulses that arise from

the full-energy, photoelectric interactions in the detection medium. Some counts also arise from

single or multiple Compton interactions that are followed by a photoelectric interaction where all

the photon energy is deposited in the detector in a short enough time to be considered a single

event. For each peak the centroid represents the photon energy E_0, and its net area above

background represents the total number of full-energy interactions in the detector and is usually

proportional to the activity, source-detector distance, and solid angle subtended of the emitting

isotope. Its width is determined primarily by the statistical fluctuations in the charge produced

from the interactions plus a contribution from the pulse-processing electronics.   If the

characteristic gamma peaks are well resolved, there is little need to evaluate the Compton spectra

for source identification. However, if the gamma peaks are not easily identifiable, additional

information can be gained from the Compton continuum.

3.2.2   Spectral Features, the Compton edge and the Compton region

In Compton scattering, the gamma ray is not absorbed, but rather scattered through an

angle θ by an electron, which recoils and carries away some of the gamma ray's energy E. (The

scattered gamma ray then escapes from the scintillator; the probability that a Compton scattered

gamma ray scatters again in a typical size scintillator like a 3x3 NaI(Tl) is quite small (1% to

10%), which means it is unlikely to detect a gamma ray that has undergone two Compton

scatterings.) The gamma ray initial wavelength is

$$\lambda = \frac{hc}{E} = \frac{1240\ nm}{E} \qquad (3.2)$$

where E is in eV. The change in wavelength is

$$\Delta\lambda = \frac{h}{mc}(1 - \cos\theta) = 0.00243(1 - \cos\theta)nm \qquad (3.3)$$

where h is Planck's constant, m is the mass of the electron and c is the speed of light. From this

equation the energy loss of the gamma ray will vary from zero (when $\theta = 0°$) to a maximum

corresponding to a wavelength shift of 0.00486 nm (when $\theta = 180°$). This maximum energy loss

is called the Compton edge. The energy distribution of Compton scattered electrons is

essentially a constant. So the Compton spectrum produced by a photomultiplier tube is an

almost flat plateau from zero energy up to the Compton edge where it drops off sharply (at a rate

limited by the energy resolution of the tube) [3]. The Compton edge is calculated by

$$hv'|_{\theta=0} = \frac{hv}{1 + 2hv/m_0 c^2} \qquad (3.4)$$

If the Compton edge is known then source energy can be calculated.

3.2.3 Spectral Features, Backscatter Peak

This peak is caused by gamma rays that have interacted by Compton scattering in one of

the materials surrounding the detector. The energy of the backscatter peak is given by

$$hv'|_{\theta=\pi} = \frac{hv}{1+2hv/m_0 c^2}. \qquad (3.5)$$

Gamma rays scattered by more than 110° - 120° will emerge with nearly identical energies in

the 200- to 250-keV range. Therefore, a mono-energetic source will give rise to many scattered

gamma rays whose energies are very close in value and result in a peak observed in the recorded

9

spectrum [4]. Next, we briefly discuss why the spectrum from a NaI and PVT detector look the way that they do.

3.3 Measured Spectra

Figures 1 (a) and 1(b) show spectra obtained from NaI scintillators and a large PVT plastic for the same five sources plotted as a function of channels [5]. Typically, the channels are converted to energy prior to conducting analysis; however, figure 1 shows the detector counts as a function of channels. Data from PVT detectors are typically processed as sums of counts above a background. The counts are either the total counts above a low-level discriminator (used to eliminate electronic noise) or total counts over a limited energy region, such as between 50 keV to 450 keV (e.g. to emphasize U-235 and Pu-239) [5].
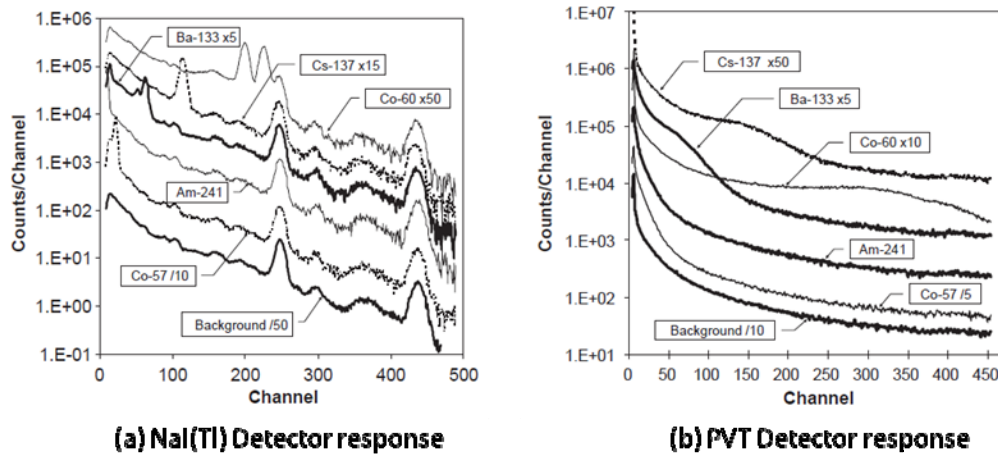
Figure 1: Measured spectra from a NaI and PVT detectors [5]. As compared to the spectrum produced by the PVT detectors, NaI detectors produce well defined peaks and register measureable differences in the Compton region that can be used to distinguish various radio-nuclides

The measured spectra show two significant differences; the most obvious is that the NaI(Tl) spectra have well-defined peaks, whereas the PVT outputs are smoother, with much less defined structure. Germanium detectors offer even better resolution than NaI(TI) but tend to be

10

smaller, much more expensive and are far less efficient than NaI or plastic detectors. Typical

resolutions of NaI(Tl) detectors are on the order of 5-10% depending on the gamma ray energy

[5]. The second major difference appears in the low-channel region where there is a significant

increase in counts in the PVT detectors compared to the NaI(Tl) detector. These low energy

counts in PVT correspond to Compton scattered events that generally appear at higher energy in

NaI(Tl) [5].

There are two important mechanisms for photon energy loss for the detectors used in this

research;   Compton scattering and photoelectric absorption (figure 2).
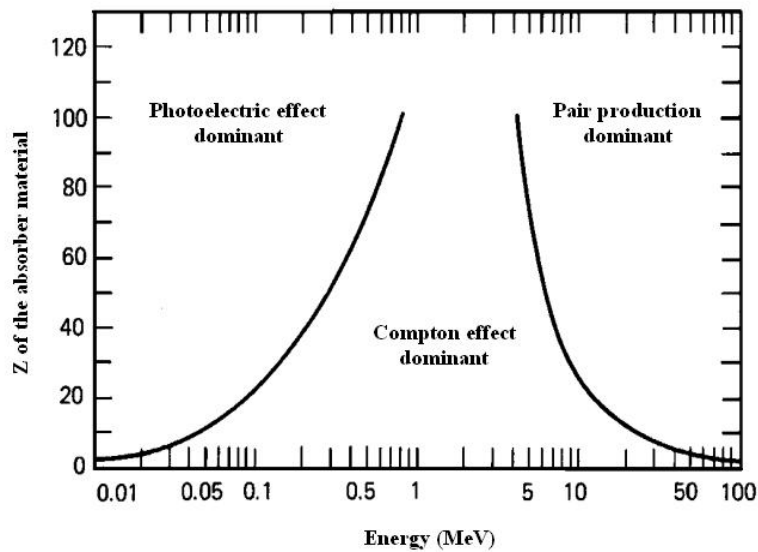
Figure 2: Regions of dominance for gamma interactions within absorbing material [4]. For the source and material interaction studied in this research, photoelectric effect and Compton effect generate the detector responses.

Rayleigh or ''coherent'' scattering is an elastic process that transfers negligible amounts

of energy, and is ignored in this discussion. Although the pair production mechanism is possible

above 1.02 MeV, its probability remains relatively low until photon incident energies reach

several MeV, and is thus of little consequence here. Over the energy range of interest for this

research, Compton scattering and photoelectric absorption dominate, and it is their interplay that determines the differences between the observed detector response functions.   The absence of peaks and the buildup of low energy counts in the observed PVT spectra indicate that Compton scattering is the dominant mechanism for photon energy deposition. This observational deduction is consistent with the energy dependence of the photon interaction cross-sections in PVT calculated from standard data.   Relative comparisons show that in PVT, Compton scattering is more probable than photoelectric absorption for incident photon energies greater than 20 keV, and totally dominates for energies greater than 80 keV because of the low average Z value in the PVT molecules. In NaI(Tl), Compton scattering does not supersede photoelectric absorption in importance until the incident photon energy exceeds ≈300 keV.   These observations are qualitative; nevertheless, they indicate important functional areas for PVT-based systems. First, because PVT's response is to shift counts to lower energies, a requirement for PVT-based systems is to have a very low value for the lower level discriminator to maximize the signal (lower than that required for NaI(Tl) due to the differences in energy deposition mechanisms). Second, even though PVT distorts the incident spectra, there are subtle variations in the PVT energy response that provide opportunities for limited spectral analysis by selecting a few broad energy windows [5].

3.4   Parametric Equation to Describe Detector Response

In mathematics a parametric equation is a method of defining a relation using parameters. A simple kinematic example uses a time parameter to determine the position, velocity, and other information about a body in motion. In this research the parametric equations relate the detector response to the "source – detector" distance from a wall and the source photon energy in a box shaped space. That is, if input *"A"* produces response X and input *"B"* produces response Y then

input ($A + B$) produces response ($X + Y$) [6]. The responses can be plotted as a function of distance and energy and fitted to generate equations that describe the detector response at a given distance and photon energy. The curve fit equations generated from three configurations of wall – source – detector describe individual detector responses from any of the walls in a room; the overall detector response can then be calculated by super-positioning of the individual detector response. For the simulation geometry in figure 3, the detector is 10 cm from wall 1, 100 cm from wall 4 and 100 cm from the lateral walls.
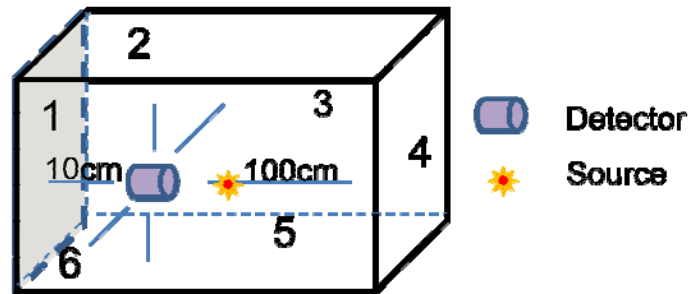
Figure 3: Proposed detection geometry to study detector response. At the depicted detector location the total response is the superposition of the responses generated from the six surfaces

The total response for the detector would be the combination of the individual detector responses calculated at 10 cm from wall #1 + 100 cm from wall # 4 + 4x responses calculated from walls 2, 3,5 and 6 (lateral surfaces) of the room. There is a possible limitation of this model; in considering individual scattering contributions from the walls, it ignores the cross-talk between the walls. That is, at a corner where two walls meet, a photon may scatter from one wall then scatter into another and then register in the detector. In order for this methodology to work it is assumed that the crosstalk from the corners of the walls has a negligible effect on the number and the energy profiles of the backscatter photons.

Once predictions from simulation fits are calculated, experiments with similar source – detector – scattering medium geometry will be conducted using a Cs-137 source and concrete walls. The results from the calculations and the experimental data will be plotted and fitted in a similar manner to the simulation data. The results should generate data that can be compared to the simulation data to determine whether the two generate similar responses.

IV.   Methodology

4.1   MCNP

Scattering is a function of material density, thickness and source energy. Gamma photons interact primarily with atomic electrons and are attenuated in proportion to the electron density and the material thickness. Source energy effects the angular distribution of scattered gamma rays as predicted by the Klein-Nishina formula [4]. MCNP can take a combination of structural materials and source energies and model photon interactions for a given simulation geometry. Scattering experiments by the Laboratory for Threat Material Detection, University of New Brunswick used MCNP to model the change in flux of scattered photons to indicate the presence of an anomaly.   The magnitude of the change was used to identify anti-personnel mines hidden in soil [7]. An isotropically emitting source in a changing geometry was modeled in the study to evaluate the detector response and to quantify the photon current at various distances.

4.1.1   MCNP Tallies

Two types of tallies are used to quantify the effects of scattering in the MCNP modeling, the F1 (surface current integrated over a surface) and the F8 (pulse height) tally. The F1 tallies the particle surface current across a selected surface. Each time a particle crosses the specified surface, its weight is added to the tally, and the sum of the weights is reported as the tally output. The tally in this study was refined by the use of the cosine cards to quantify the photon current in the positive and negative directions. This was particularly useful earlier in the research to develop an intuition for backscattering. As shown in figure 5 the tally surfaces are depicted using dashed lines where particles are tallied using the cosine cards. The incident photons are

tallied by the cosine (0 – 1) cards and the backscattered photons are tallied by the cosine (0 – (-1)) cards. Comparing the results of the two cosine tallies can quantify the fraction of the total particle current that is generated from the scattering medium.

F8 tally is the pulse height tally. It is the collective history weight deposited in the detector [8]. When used with energy specification cards it provides the energy distribution of pulses created in a detector. The energy deposition algorithm simulates the response seen in a physical detector, and is determined by subtracting the photon energy outflow from the photon energy inflow in the detector volume. The output is given in terms of counts per bin.

MCNP is very useful for predicting photon interaction but MCNP cannot completely replicate the photon interactions for a given detection problem. The experimental configurations are often vastly more complex and with many more variables than can be modeled in simulations; as a result the simulation results never completely match the experimental results. Figure 4 illustrates this difference. A Co-60 source was counted by a high purity germanium (HpGe) detector and a simulation of that experiment was modeled in MCNP.
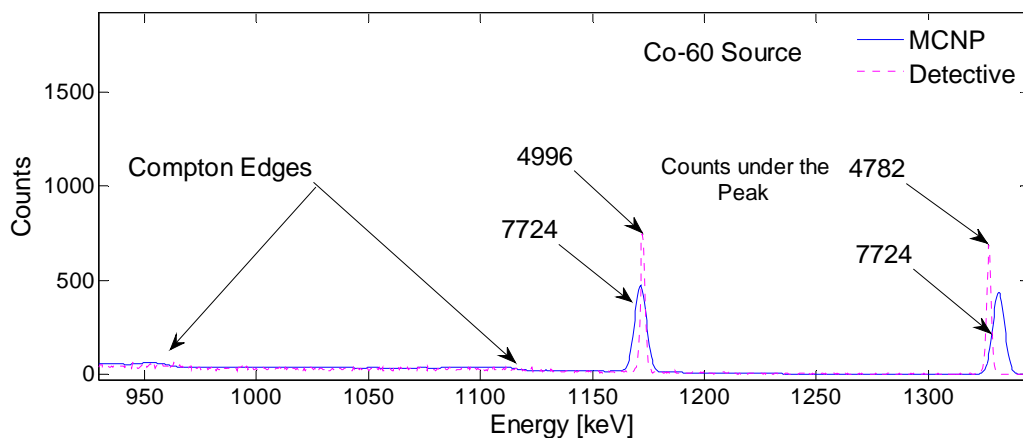
Figure 4: Comparison of MCNP and HPGe detector generated spectrums from a Co-60 source. The peak areas represent the integrated counts under the peaks from the detector and the model. Though in agreement, the responses are not the same.

16

The results show that model and experiment are in good agreement overall, but in this case simulation calculations overestimate the results produced from the HPGe detector. A way to ensure that similar data are being compared is to simulate the data until the relative errors are of similar values. As an example if the relative error in the experimental data is 5% in the 100 keV energy bin (for a given source-detector geometry) then the simulation must run enough particles so that after solid angle adjustments, background count subtraction, and the energy binning, 5% relative error is also achieved in the 100 keV energy bin.

4.1.2   F1 Tally Experimental Design

Figure 5 illustrates how the simulation geometry was defined. In this case a 15 cm x 45 cm x 180 cm space with a 600 keV isotropically emitting source was placed 100 cm from the concrete wall.   An F1 tally with a cosine tally multiplier card was used beginning at the concrete surface and at surfaces at increasing distance in 10 cm increments. The results provided backscatter as a function of varying distance and source energy at the tally surfaces.
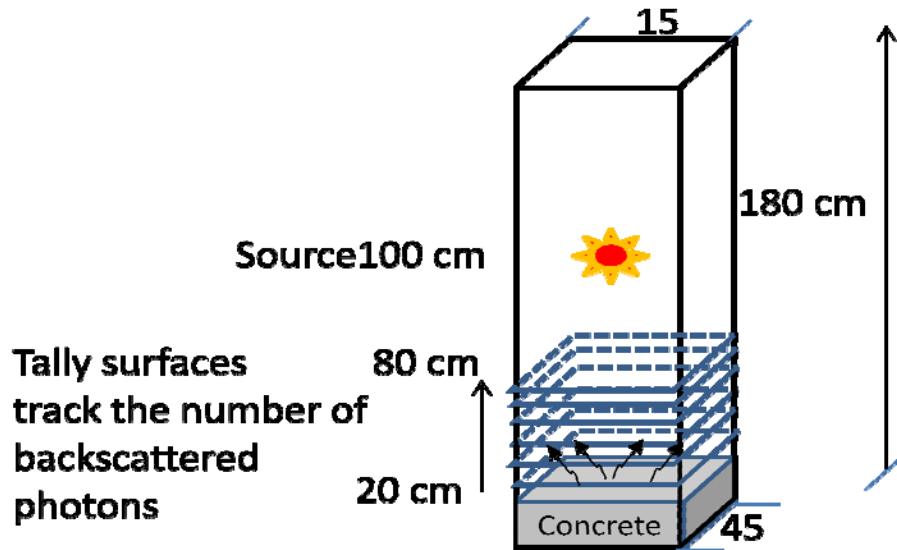
Figure 5: Depiction of the MCNP model designed to study backscatter using the F1 Tally. Tally surfaces begin at 20 cm and increase in 10 cm increments. Tally surfaces were modified to report backscattered photons from the concrete wall.

The Klein-Nishina formula predicts that as source energy increases fewer photons are scattered in the reverse direction, therefore, using 1200 keV source should provide much less backscatter than using a 600 keV or a 200 keV source. In addition to the reduced backscatter, the amount of photons at the tally surfaces was expected to drop as a function of distance. Even though the mean free path (MFP) for all backscattered photons is in 10s of meters (in air), due to the limited geometry of the model and the isotropic directions of the scattered photons, a significant number of particles were expected to get lost between the concrete wall and the tally surface.

4.1.2.1 F1 to model backscatter as a function of varying wall thickness

In order to determine the effect of the amount of material on the backscatter, varying thickness of scattering material were studied. It was assumed that there was a threshold thickness for generating maximum backscatter photons beyond which there was no additional

benefit to the amount of backscatter. Also, as material thickness became greater than the photon

MFP in the scattering medium, larger numbers of photons were expected to be absorbed in the

material. To determine this thickness, the depth of the concrete wall was doubled, beginning at 5

cm until the amount of photon backscatter stabilized.   Also, to study the effects of material of

different density, the model was reconfigured with varying thickness of steel from 1 cm to 5 cm.

It was expected that steel would absorb more photons and have a thinner threshold thickness.

The sample F1 tally MCNP input file is shown in appendix A and the photon MFP for three

sources of energy in concrete and steel is shown in appendix G. Next the pulse height tally was

used to further study backscatter.

4.1.3   Modeling detector response in MCNP using the F8 tally

The F8 tally is the pulse height tally. The pulse height tally is analogous to a response

from a physical detector and provides the energy distribution of pulses created in the designated

cell. The simulation space (figure 6) was a 4 meter x 3 meter x 2 meter concrete box with a

source and a detector in constant geometry. The cell tally was modified using an energy card

dividing the pulse height into energy bins corresponding to the total energy deposited in a

detector by each physical particle history [9]. The model only accounted for the concrete

features of the experimental area. Features such as HVAC ducting, the laptop and the desktop

computers were not modeled because scattering and attenuation from those features was assumed

not to contribute significant photon scattering when compared to the large concrete walls.

The models also assumed negligible effects due to the environment and did not account

for temperature shifts or additional materials from the surrounding environments. Finally it

assumed maximum scattering with the model's 20 cm thick concrete walls. The entryway door

made of thin steel, wood and glass was also not modeled because it was more than 2.5 meters away from the detector and the source.

In the simulation the source and detector unit was maintained in a constant co-linear geometry and moved from the wall in 10 cm increments (figure 6). The distances from the lateral surfaces remain constant and the only variable was the distance from the front wall to the NaI(Tl) cylindrical detector.
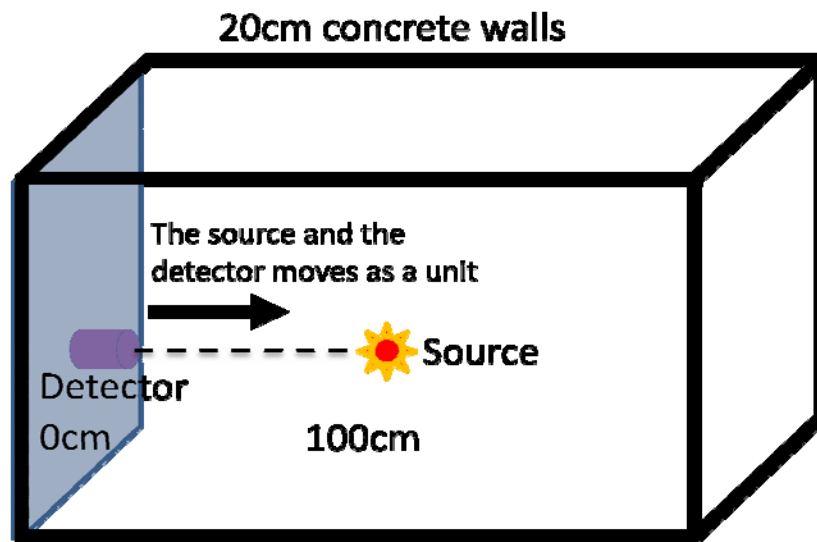
Figure 6: The 3x3 NaI detector and the source are placed in the middle of the simulation space and are moved away from the vertical wall on the left in 10 cm increments. The distance from the lateral walls remains constant.

Mono-energetic, isotropically emitting photon sources from 200 keV to 1200 keV in 100 keV increments was modeled to determine the detector response over a broad range of photon energies. 1×10^8 particles were simulated for 200 keV, 600 keV, 662 keV, and 1200 keV and 1×10^7 particles were simulated for 300 keV, 400 keV, 500 keV, 700 keV, 800 keV, 900 keV, 1000 keV, and 1100 keV photon energies. The lower particle count took nearly 1/10th the time

while providing comparable detector response (but with much larger counting errors). The larger

count models took approximately 23 hours to run three simulation geometries for one

configuration. The total run time for the entire configuration run at 1×10^8 particles across all

photon energies would have taken too long therefore, it was assumed that if the lower particle

counts had been modeled at 1×10^8 particles, the relative error would have been the same as

the relative error for the larger particle simulation ($5 \pm 2\%$ in energy bins below the Compton

edge for the Cs-137 located at 477 keV). A sample input file for the MCNP model is shown in

appendix A. Next, an experiment to replicate the simulation models was conducted in order to

compare the model to the detector response and verify the contribution from scattered photons on

the NaI detector.

4.2 Experimental Verification of the Contribution of Scattered Radiation on 3x3 NaI
Detector Response

Similar to the simulations to study the particle current and the pulse height tallies, photon

interaction as a function of detector distance was studied by moving the detector away from the

scattering medium and by comparing net interaction counts within established energy windows.

The net interaction was defined as:

$$\text{Net Interaction} = \text{Gross counts with wall} - \text{Gross counts without wall} \qquad (4.1)$$

The energy window for comparing the responses was set from the detector responses

generated from 100 keV to 350 keV. Those particular energy boundaries were chosen because

all of the backscatter peak energy values fall well within those two values and any change in the

detector response due to geometry changes or any other variables would be apparent within those

boundaries.

4.2.1 The Experimental Set Up

The experiment was conducted in room B01, Building 470. The room is a concrete structure with at least 20 cm of concrete in all six planes except in the doorway leading in to the space. The room offered a rectangular geometry that was easily replicated in MCNP (figure 7).
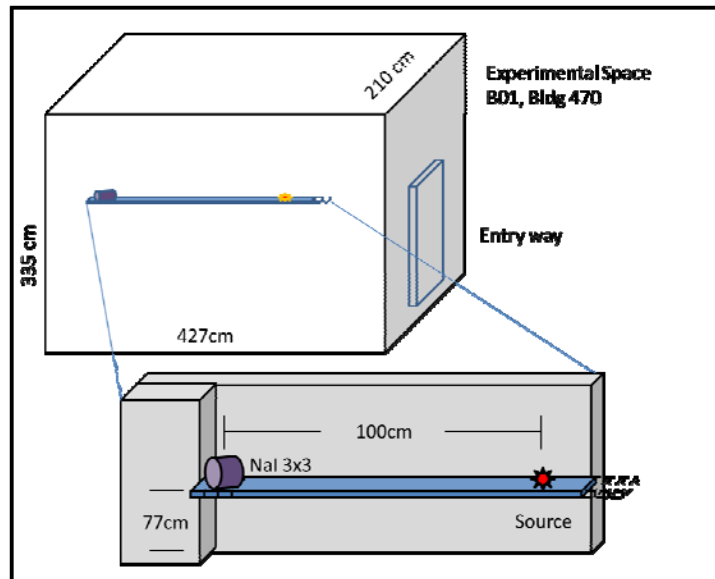
Figure 7: Description of the experimental space. The detector and the source are kept in a constant geometry using a thin wooden plank. Both are moved back as a unit in 10 cm increments.

Similar to the MCNP model, the source and detector remained in a constant co-linear geometry and the distance from the lateral surfaces remained constant. The source and detector unit was moved from 0 cm to 100 cm in 10 cm increments while Gamma Vision software recorded the detector – photon interaction. The spectrum was expected to should show an initial increase in photon counts and a gradual drop until the response flattened out. The experimental

22

room composition was mainly concrete and it was assumed that when compared to the scattering

from the concrete, any other materials did not contribute significant amounts of scattering.

4.2.2 Equipment

4.2.2.1 3x3 NaI(Tl)Detector

A 3x3 cylindrical thallium doped NaI crystal with a flat faced cylindrical geometry

allowed the detector placement flushed with the wall (figure 8).

Figure 8: 3x3 NaI detector with pre-amplifier in the experimental configuration

NaI(Tl) detectors offer sufficiently high resolution and can identify radionuclides based

on the characteristic gamma spectra [10]. The absolute efficiency of the detector ranges from

0.1126 at 122 keV to 0.314 at 662 keV source at 2 meters. Typical resolutions for NaI(Tl)

detectors range from 15.08% at 122 keV to 8.06% at 662 keV [10]. A disadvantage of this type

of detector is the fluctuation in the gain as a function of temperature; therefore a gain stabilized

amplifier was utilized along with the detector. The hardware was controlled using the ORTEC

Gamma Vision software which also provided a histogram of real-time photon interaction in the

detector. Once the data was gathered it was evaluated using MATLAB software. The energy

calibration calculations are presented in Appendix E of this document

4.2.2.2 Plastic Scintillators

A plastic scintillator consists of organic scintillating molecules in a polymerized matrix.

Plastic scintillators are characterized by a relatively large light output [typically 25-30% of

NaI(Tl)] and a short decay time, on the order of a nanosecond.
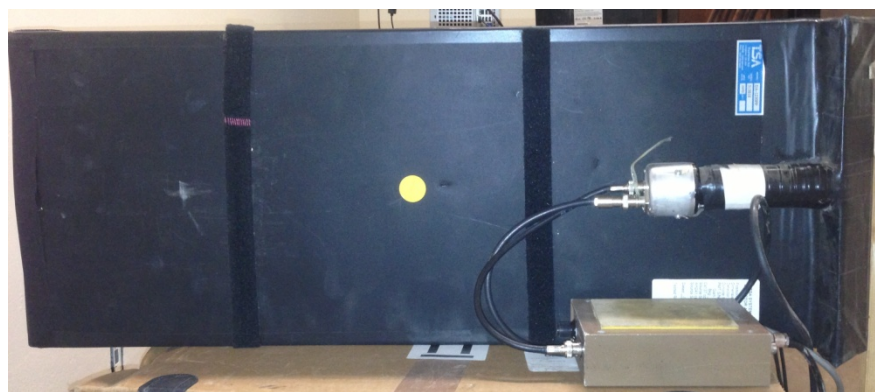
Figure 9: Large plastic scintillator with PMT and pre-amplifier in the experimental configuration

This makes the material well suited for fast timing measurements [11]. Plastics are often

used for detection of charged particles, or when large-volume solid scintillators are needed.

Because of the low density and atomic number, plastic scintillators are not suited for gamma ray

spectroscopy; they can and do interact with gamma particles but cannot provide well defined

peaks (figure 1b). The plastic detector used in this work is a single sheet of polyvinyltoluene

(PVT) measuring approximately 30" x 12" x 1.5" (figure 9). The specific model was the DA-

1230pp manufactured by TSA Technologies in October 2002. Data from the PVT detector was

processed as sums of counts (also called ''gross'') of all counts above a 20 keV low-level

discriminator (used to eliminate electronic noise).

4.2.3   Background, Relative Error and Counting Time

A goal of achieving a relative error of approximately 5% ± 2%, in the NaI detector net

backscatter counts was deemed acceptable. The counting time to achieve the desired relative

error was determined by the relative error formula,

$$\sigma = \frac{\sqrt{n}}{n} \tag{4.2}$$

where n was the number of net photon counts at 360 keV. Assuming the background count

remained approximately the same over the experimental area, the results of the net count for a 20

minute counting window produced n = 235 counts and a σ = 6.5% which was within the

acceptable goal for conducting the experiment.

4.3 Developing a Parametric Equation to Predict Detector Response

Once the three wall – detector experimental geometries were modeled in MCNP

[Appendix B – D] and the photon interaction were tallied in the detector volume using the pulse

height tally, the source and the detector were held in a constant geometry and the scattering wall

was moved in 10 cm increments up to 100 cm in the three configurations (figure 10). 100 cm

was chosen as the maximum distance based on preliminary analysis of the amount of

backscattered photons at that distance. The initial F1 tally experiments suggested that only 4%

of the backscattered photons generated by the scattering medium were present for interaction

with the detector surface at 100 cm.
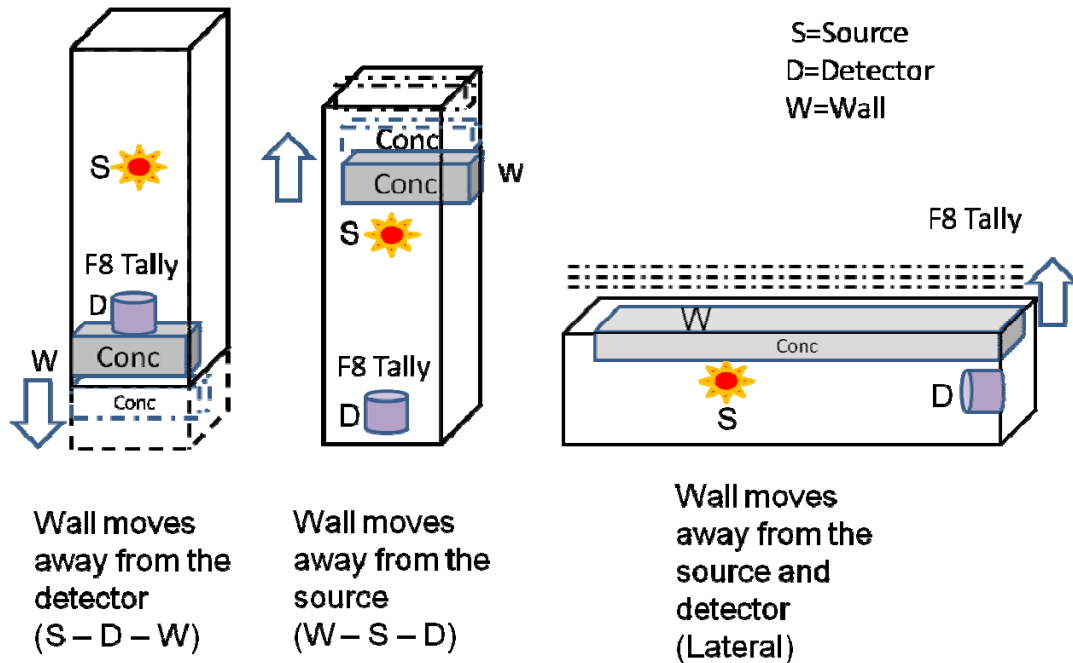
Figure 10: Three configurations of Source – Detector and concrete scattering medium geometry. Each one simulates the geometry required to produce scattering from only one wall in a box shaped space.

The first configuration modeled the scatter from the wall in front of the detector plane from 0 cm to 100 cm. The next configuration modeled the scattering contribution from the wall that was on the opposite side of the detector. This modeled the wall next to the source and moved it away to 100 cm. The final configuration accounted for the scattering contributions from the lateral walls that completely covered the source – detector unit from 0 cm to 100 cm.

The individual backscatters from the configurations in figure 10 only represent the scattering contribution from one wall within the box. The overall detector response is the superposition of all the individual responses from the six walls in the boxed shaped space as shown in figure 11.

Figure 11: Concept of superposition: Individual scattering from the six walls describes a portion of the overall detector response. When combined together the six individual responses make up the total response.

The individual detector responses from the walls was integrated over the energy windows from 70 – 370 keV and plotted versus distance for the three configurations. These resulted in two dimensional plots that mapped the detector response from 0 cm – 100 cm. The plots were fitted using the MATLAB curve fitting toolbox and the fit equations were catalogued under their respective configurations.

The total response functions were calculated by combining the individual responses from the six scattering contributions of the detection space as shown in figure 11. The total response (R_{total}) was calculated by adding all six of the individual wall contributions.

Using this methodology, the combined response could be calculated for any given position within the experimental space.

Next, to generalize the prediction methodology so that it predicted not only the response as a function of distance but also the response as a function of energy, the detector responses were plotted versus distance and energy. Using the integrated detector response results from 200 keV to 1200 keV, surface plots were created that map the detector response over the energy ranges. The MATLAB surface fit tool was used to fit the data and generate fit equations for the three configurations. The three fit equations describe the detector response for the S-D-W, Lateral Wall, and the W-S-D configurations over distance and energy.

4.3.1 Verification of Calculated Response with Model and Experimental data

The calculated response is compared with MCNP modeled data as well as the experimental data. The calculated detector response from each of the walls (at the appropriate distances) will be determined using the fit equations from the 2 dimensional and the surface plots. The total response will be determined using the sum of the individual surface responses.

V. Results

5.1 Results of Determining Scatter and Photon Current using MCNP F1 Tally

The goal of the study was twofold; first to understand the intensity of the backscatter photon current from the scattering medium as a function of distance and material thickness and second to understand the effects of source photon energy and material thickness on the energy distribution of the backscatter photons. The simulation geometry was depicted in figure 5, section 4.2.1. It was determined that as the distance increases between the scattering medium and the tally surface, the photon current falls to 42% of the maximum backscatter at 10 cm to approximately 5% of the maximum backscatter at 60 cm (Table 2).

Table 2: As the distance from the wall increases, the amount of backscatter drops significantly

Distance	Fraction of simulated particles	Error	% Max Backscatter
0	9.29E-04	1%	100%
10	3.86E-04	2%	42%
20	1.98E-04	2%	21%
30	1.16E-04	3%	13%
40	8.01E-05	4%	9%
50	5.94E-05	4%	6%
60	5.10E-05	4%	5%

The primary tool to evaluate the backscatter was the F1 (surface current) tally. Taking the F1 tally at the surface with the cosine (-1 0) card provided a tally of the photons travelling in the opposite direction to the photons coming from the source. Table 2 presents the fraction of the maximum backscatter as a function of distance away from the wall. That is at 0 cm tally surface backscatter was the highest possible in that simulation geometry, and the other results are

calculated as a fraction of that maximum. The data shows that there is a substantial drop in the backscattered photons over the distance range.

The drop in the amount of backscattered photon with increasing distance was expected but the backscatter dropped unexpectedly fast over the 60 cm. This was unexpected because the MFP for a 600 keV photon (in air) is greater than 100 meters and one should expect to see larger amounts of backscattered photons within 100 cm of the scattering medium. An explanation for this behavior is that the wall is not a point source but a planar source emitting photons in a 2π steradians with equal probabilities, therefore a photon at the edge of the concrete wall with even a slightly outward angle is likely to travel out of the simulation geometry. At 60 cm away from the wall far more photons have traveled out of the simulation geometry therefore fewer backscatter photons interact in the detector. An additional simulation that modeled the wall as a point source resulted in 59% to 6% of the maximum backscattered particles for the same geometry. When compared to the planar geometry of the model with a range of 42% to 5% the maximum backscatter results don't seem unreasonable. But the geometry in the simulation was relatively small and the results from this study prompted further exploration to understand the effect of increasing the scattering medium surface area on the amount of backscatter registered. The simulation geometry was changed such that the scattering surface and the tally surfaces were made 10 times larger. The tally surface distance, however was kept at the same. The results are presented in figure 12.
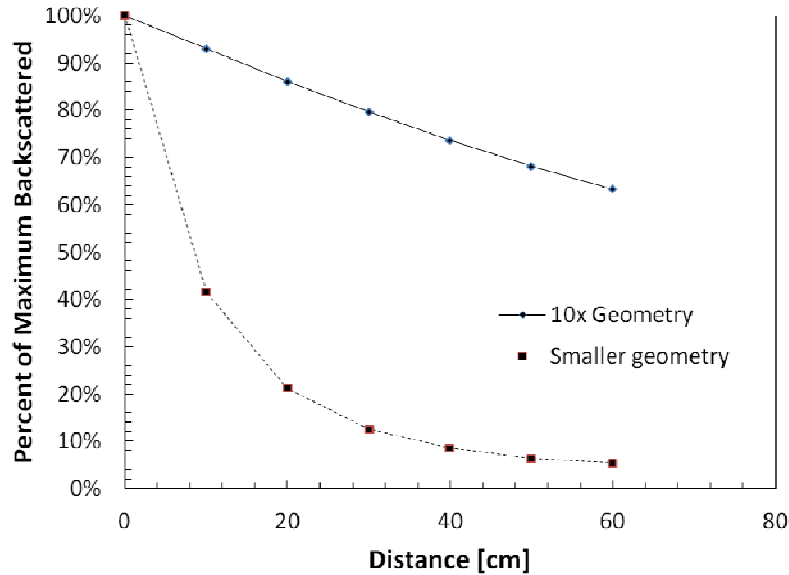
Figure 12: Percent of maximum backscatter as a function of distance for two geometries

As the surface area increases, the percent of maximum backscatter increases (over the same distance). The response behaves almost linearly but this is probably due to the large ratio between the detector compared to the wall area rather than a linear relationship between the two. The smaller geometry displays an exponential like decrease rather than the expected decrease by a power function.

An interesting comparison is also to look at the ratio of the surface areas to the tally distance for the same geometry. The surface area to tally distance ratio is (675 cm^2:60 cm) but for the larger geometry the same ratio is (67500 cm^2:60 cm). The results show that as the distance from the scattering surface becomes a smaller fraction of the tally surface area, the drop in the detector response becomes less drastic. This is likely due to the solid angle difference between the smaller and the larger detector – wall geometry. An attempt was made at generalizing the backscatter behavior as a function of distance that could describe the detector response regardless of the scattering wall surface area or the solid angle between the two. This was accomplished by normalizing the detector responses with the solid angles at the appropriated

32

distances from the scattering wall. However, the results failed to show similarities in their behavior over the distances modeled in the simulation. There has to be a general relationship between the detector response and the surface area of the scattering medium but unfortunately this was not extracted from the simulation geometry.   Thus a recommended simulation for follow on research is to use a large simulation geometry, the wall size could be varied from very small to very large while keeping the detector in one place; this would provide detector response as a function of solid angle that could be analyzed for a trend in the detector response. Then, the experiment could be repeated at various distances from the scattering wall to generate the response behavior as a function of distance. Analysis of this data should result in generalized prediction of backscatter response for any detector and scattering wall size. At this point the comparison between the responses for the two geometries simply show that as the scattering wall surface area becomes much larger, the detector registers many more backscattered photons. Results from the larger geometry are probably the reason behind the increasing use of large plastic detector (larger than 1.5 meters) and larger NaI detectors by the Department of Homeland Security at the U.S. border crossing points; simply because larger detectors register many more photons. But for the purpose of this study, the results from both geometries suggest that in order to maximize the benefit from backscattered photons, the detectors need to be employed closer to the scattering surface rather than at farther distances. Next the results of the study to understand the effects of varying the wall thickness on the particle current as function of distance for two materials is presented.

5.1.1   Backscatter as a Function of Wall Thickness

This study modeled the backscattered photons as a function of wall thickness (in MCNP). It was discovered that a threshold thickness of 15 cm of concrete and 3 cm of steel backscatters

the maximum number of photons. Maximum backscatter was defined differently in this simulation. Using the same geometry in figure 5, section 4.2.1 (over 200 keV, 600 keV, and 1200 keV source photon energy) the percent backscattered represents the fraction of inbound photons at 0 cm from the scattering concrete wall. The results are presented in Table 3.

Table 3: Percent of photons backscattered as a function of wall thickness. Threshold thickness for generating backscatter is reached shortly after 15 cm for a concrete scattering medium.

Percent Backscattered					
keV	5 cm	10 cm	15 cm	20 cm	25 cm
200	24.71%	26.69%	26.79%	26.80%	26.80%
600	18.90%	22.95%	23.52%	23.60%	23.60%
1200	18.42%	17.44%	18.28%	18.42%	18.45%

As source energy increases fewer and fewer photons are backscattered. This is in agreement with the predictions from Klein-Nishina formula. In all three cases the threshold thickness for concrete remains the same at 15 cm.

In order to show the effect of denser material on the amount of backscatter, a mid range energy source was modeled with varying thickness of steel. Since steel is denser, the thickness was changed in smaller increments (from 2 mm to 1 cm in 2 mm increments and from 1 cm to 5 cm in 1 cm increments). Comparison of the photon behavior of steel and concrete at 600 keV are shown in figure 13.
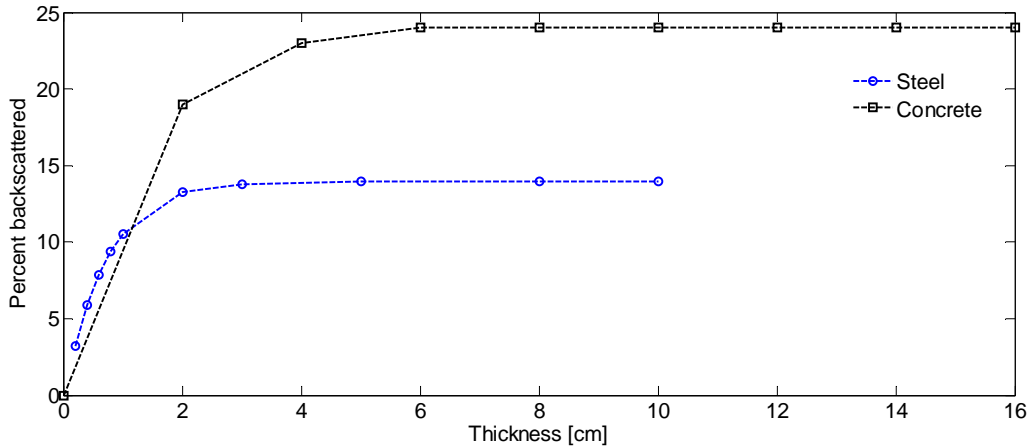
Figure 13: Threshold thickness for maximum backscatter using steel wall is reached at 5 cm as compared to 15 cm for concrete.

Much smaller thickness steel is needed to achieve maximum backscatter. The maximum backscatter is also less than what was scattered using a concrete wall. In the concrete experiment approximately 20% of the incident photons are backscattered where as only 14% are backscattered using steel. The difference in backscatter using denser materials is that denser materials like steel absorb many more photons in much less thickness than less dense materials like concrete. In a detection problem, this means denser materials may either enhance the backscatter using a lot less material or absorb more photons and thereby reduce the total number of backscattered photons. More simulations using materials of different densities along with varying energy photons should be conducted to determine how material densities affect the amount of backscatter generated as well as the threshold thicknesses for generating maximum backscatter.

5.1.2   Energy Distribution of Scattered Photons

Once the effect of the varying material properties was quantified, the energy characteristic of the backscattered photons was evaluated as a function of source photon energy.

35

The goal was to determine the region of the spectrum where the effects of changing photon energy would be most apparent. The simulation tally parameters were changed to model the energy distribution of the photons scattered from the concrete wall. The source photon energy was increased from 200 keV to 1200 keV in 100 keV increments and the peak energies of the backscattered photons were plotted as a function of source photon energy. The results are plotted in figure 14 and the graph shows that regardless of the source photon energy, the backscatter energy is deposited mainly in the 100 keV – 350 keV range.
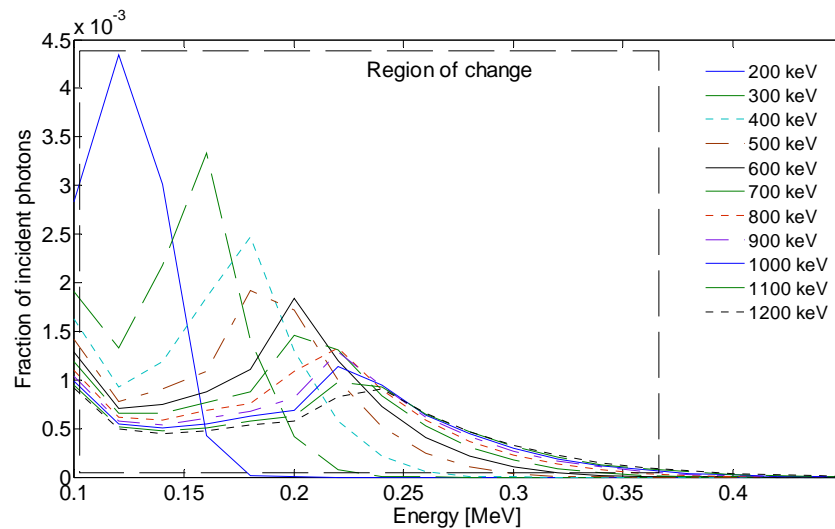
Figure 14: The backscatter photon peaks make up a region of the spectrum where changes in the spectrum are most apparent. The region spans from 100 keV to 350 keV.

This information is useful because it establishes the energy window for evaluating the effects of changing materials or energy variables. This region of evaluating change primarily consists of the photon backscatter peaks as predicted by the backscatter peak equation (3.5) over which the effects of scattered photons from the concrete wall are evaluated.

The F1 tally served as a vehicle to understand backscatter using very simple geometries but what happens when the detection problem is completely modeled in MCNP? The next section studies the detector response using a complete MCNP model.

5.2 Modeling Detector Response Using a Complete MCNP Model

In order to compare the MCNP predictions to the observed response a simulation of the physical experiment was modeled using the simulation geometry as depicted in figure 6 section 4.2.2. Using a 662 keV isotropically emitting point source to model a Cs-137 source and 20 cm thick concrete walls the simulation modeled detector response from the backscatter photons as a function of detector distance from the wall. The results were integrated over the energy window, normalized and plotted as a function of distance. The result is presented in figure 15.
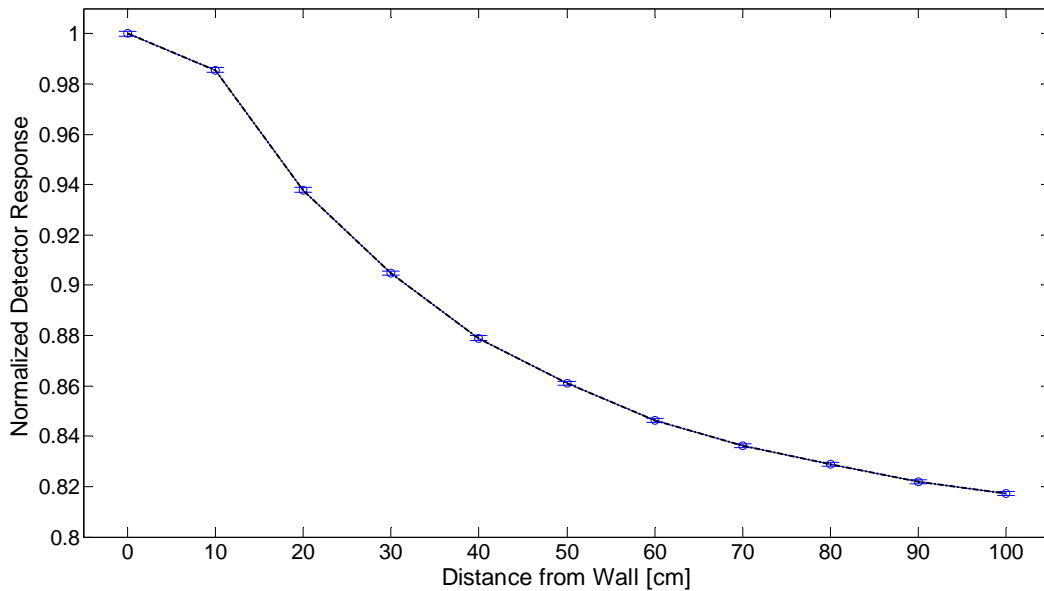
Figure 15 MCNP predicted detector response as a function of distance; relative errors range from 0.5% to 0.8%

The response represents a net response due to the effects of scattering after the direct photon interaction from the source has been subtracted. As expected the counts due to scattering decrease as the detector moves away from the wall. The results are compared to the observed results in section 5.4.2 . The results generally agree with the results discussed in the previous section but how do they compare to the experimental results? Section 5.3 presents the results of the experiment as well as a comparison of the experiment to the modeled data.

5.3   Experimental Results

The experiment used the source detector geometry depicted in figure 7, section (4.3.1). The source – detector unit was moved from the wall in 10 cm increments as the spectrum from the NaI and the plastic detector were collected at each location for 20 minutes. Another spectrum taken at 150 cm served as the baseline measurement meant to account for photon contribution from the source and background. The 150 cm detector distance was chosen as the baseline photon contribution for two reasons. First the background was constant at all distances in the experimental space so subtracting the background at 150 cm rather than 100 cm or 50 cm wouldn't have affected the net results. Secondly, as discovered in the simulation results for the larger geometry in figure 13, section 5.2, 70% of backscattered photons from the scattering medium were available for interaction at 60 cm. Since the photon current drops by a power function, it was assumed that at 150 cm detector distance the number of backscattered photons available for interaction was negligible. Next, to evaluate the data over the region of change as, established in section 5.2, the data was integrated from 70 keV to 370 keV to capture of all apparent change in the histograms. The energy window was 80 channels wide and provided slightly less than 4 keV per window resolution on the histogram. The integrated counts at each incremental distance were plotted versus distance from the front wall. The results from the NaI

detector is presented in figure 16. The results from integration count from another energy window over 370 keV – 670 keV are also shown, but the changes are less pronounced so they are not evaluated in this experiment.
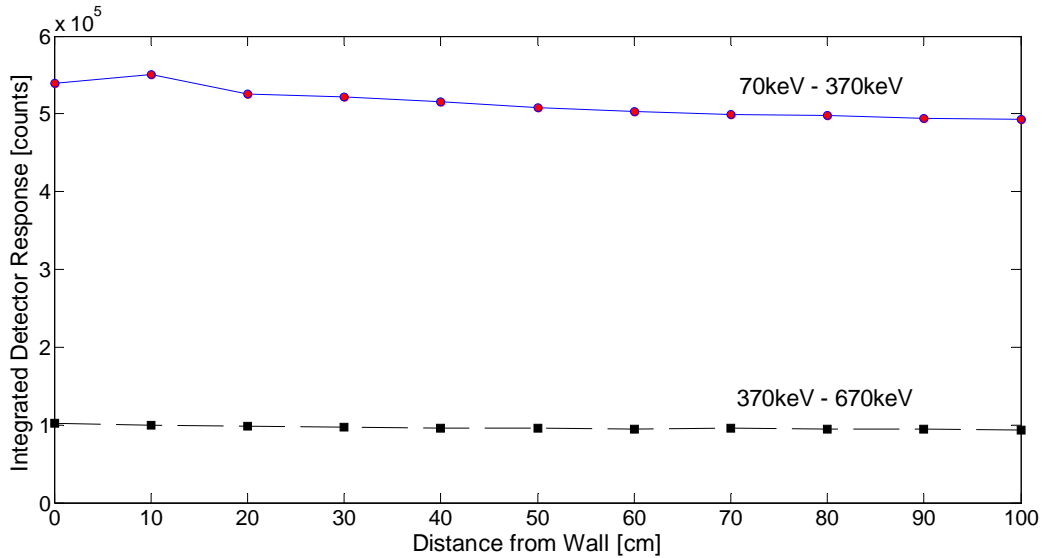
Figure 16: The integrated NaI detector response over two energy windows shows that there is variation in the response in the 70 keV to 350 keV energy window. From 350 keV to 670 keV the detector response is flat ($9.96x10^4$ counts at 10cm and $9.29x10^4$ counts at 100cm) indicating little change in the response as a function of distance.

The photon backscatter increases from 0 cm to 10 cm and gradually decreases after 10 cm. The trend is slightly different over the first 10 cm than the MCNP predicted detector response shown in figure 15 but the difference can be explained. As the detector moves away from the wall, the front face of the detector becomes exposed to a larger surface area than when the detector was in direct contact with the wall. The exposure from the source remains constant as the detector and source move away from the wall. Furthermore, the sides of the detector surfaces are exposed to almost the same amount of the surrounding surface areas at 0 cm as they

are at 100 cm so the rise in the response can only be due to the increased exposure due to the

backscatterat at the detector front face.

5.3.1 Comparison of the NaI and PVT Response

Normalized results from the plastic and NaI detectors are presented in figure 17. Whereas the NaI counts were integrated over an energy window, counts from the plastic detector were integrated over all channels. Relative errors were calculated using error calculations as described by equation 4.2 and propagated using the methods described for propagating errors for sums of counts by equation 5.2 [4].
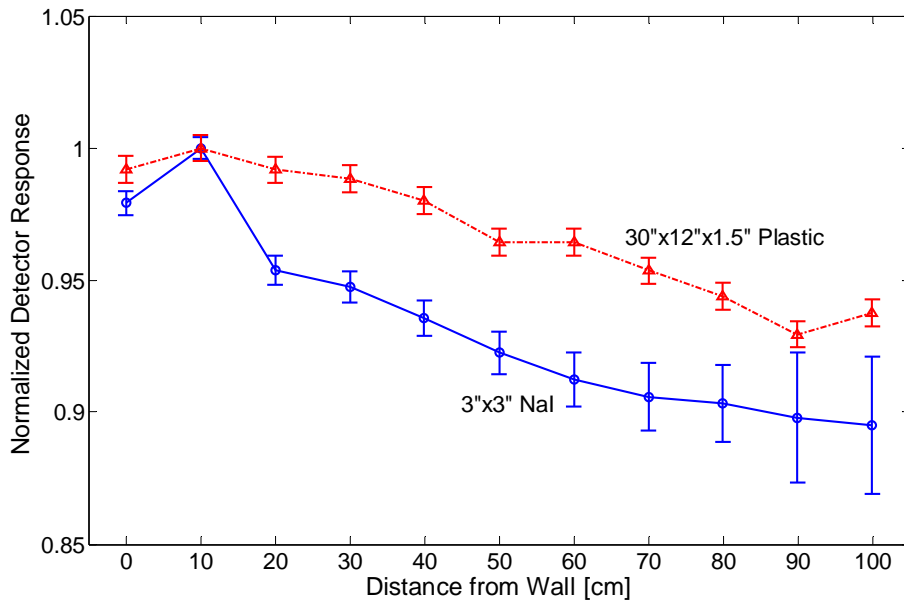
Figure 17: NaI and Plastic detector response due to the backscatter from a concrete scattering medium using a Cs-137 source.

The plastic detector is similar to the NaI results in that the detector response rises for the first 10 cm and then decreases. But the decrease over the range of distances is less pronounced, changing from 99% of the maximum at 30 cm to 94% of the maximum at 100 cm. This result

was more in agreement with the larger geometry F1 tally results discussed earlier in section 5.2. A larger detector response was expected for plastic detector than the NaI since the plastic detector is more than 40 times larger. Also, due to its larger size, the change in solid angle from 0 cm to 100 cm is smaller compared to its cross sectional area so the change from 99% - 94% over 100 cm is not that surprising.

5.3.2   Comparison of Experimental and MCNP Modeled Data

Figure 18 shows that the model generally underestimates the detector response in all but one case. The drop in photon counts is also more gradual in the experimental results whereas the modeled backscatter count drops more rapidly, especially between 10 and 20 cm. Comparing the backscatter at 100 cm shows that 89% of the maximum backscatter registers in the detector versus the 82% predicted by the model.
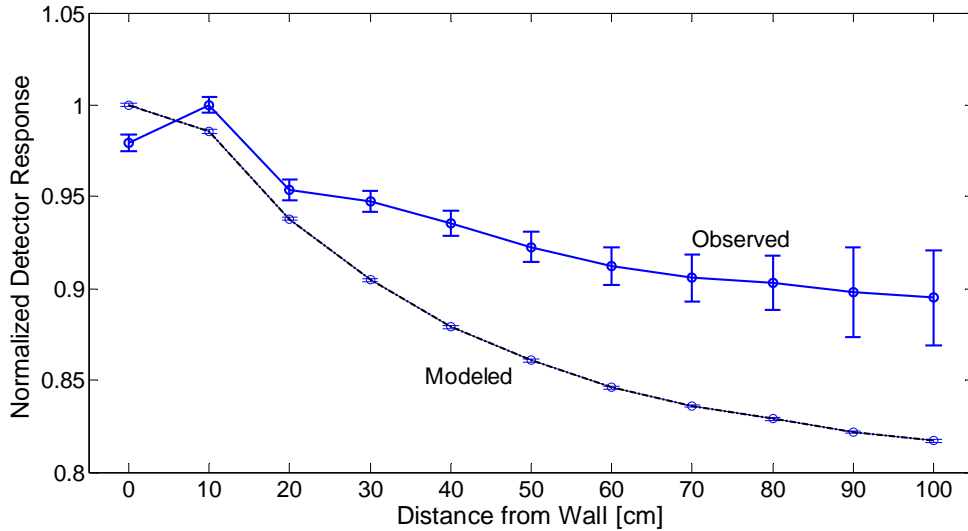
Figure 18: Modeled and experimental detector response from a 3x3 NaI detector and Cs-137 source. The responses are in agreement from 0 cm – 20 cm but become increasingly different as the detector distance from the wall increases.

The difference in the behavior is most apparent beyond 20 cm and especially at 100 cm

where there is an 8% difference between the two values. There are some possible explainations

for the differences in the responses. The two methodologies were obviously different; the

experimental geometry was vastly more complex than the simulation. However a more

insightful reason for the difference becomes apparent if we plot the detector counts versus

energy for the NaI detector and the MCNP predictions (figure 19).
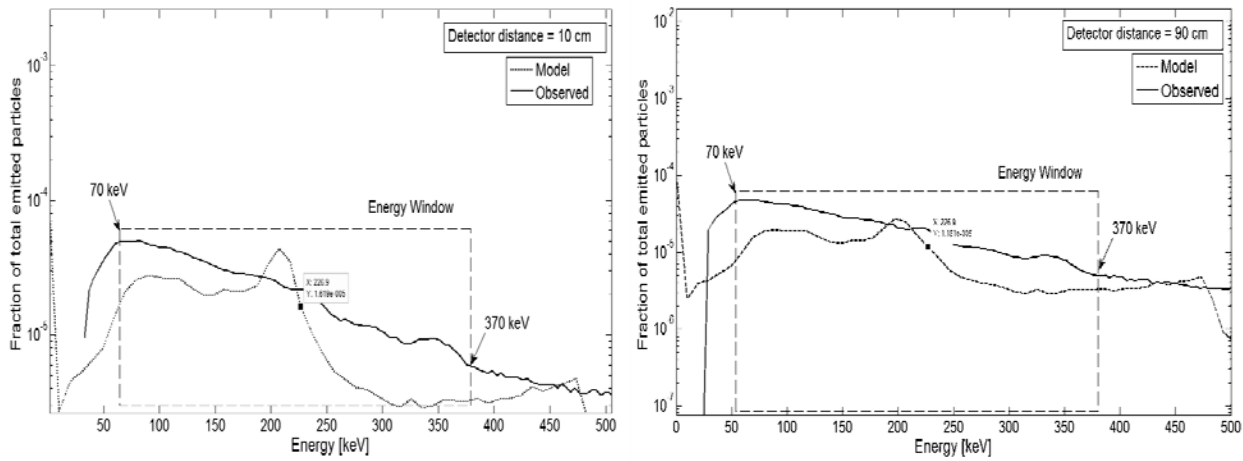
Figure 19: Comparison of the fraction of the total emitted particles that registered in the simulation and in the detector from a 662 keV photon source (for detectors at 10 cm and 90 cm from the scattering wall). The modeled response was not broadened using Doppler broadening.

The modeled response was plotted from the direct output from the simulation, which

provided the tallied detector responses as the fraction of total emitted source photons. The

experimental spectrum was normalized by dividing each value by the total number of photons

emitted from the source during the time of the experiment and resulted in the fraction of total

emitted photons from the Cs-137 that registered in the detector. By comparing these results in

this manner allowed for a direct comparison of the fraction of total emitted particles in both

methods. In general the values predicted by the model in the energy windows do not match the

observed values and therefore imply that the model did not simulate the experiment correctly. The model did not account for many small experimental variable inherently present in an experimental space. For example, the experiment was conducted in an area where there was known interference that may have coupled into the detection system circuitry. Environmental factors like temperature shifts may have affected the detection system but were not modeled in the simulation. The detector was probably affected by high frequency noise; the effect of which is generally to broaden the peak recorded in the differential pulse height spectrum [4]. Some of these effects could have been accounted in the model if the modeled data was broadened using Doppler broadening but that was not accomplished. Furthermore, MCNP simulations occur over a closed geometric system where the particles are tracked within the defined boundaries only; once outside the photons are no longer tracked. In real systems backscatter from beyond the room wall are a real possibility and may contribute to elevated detector counts. Due to time constraints these factors were not explored in detail but it is likely that a combination of these factors caused the observed and the modeled to be different from one another.

A noteworthy feature in the plots is the apparent backscatter peak in the modeled data at approximately 200 keV. The backscatter peak is significantly higher value at 10 cm than at 90 cm. This phenomenon suggests that the change in the backscatter is most apparent in the backscatter peak region than anywhere else in the energy window. Since the peak is not apparent in the observed data, it is difficult to determine if the same phenomenon was present in that dataset as well. But, it is likely that the backcatter peak was merely absorbed in the higher count Compton region of the observed spectrum.

In any case, the results show that there is agreement at 10 cm and 20 cm. The results also suggest that to maximize the counts in the Compton continuum, it is best to place the

detector approximately 10 cm from the wall. Also, in both cases at least 80% of the maximum

backscatter is still present at 100 cm. If one is going to develop a detection and identification

methodology using the backscatted photons then 80% backscatter presents a significant amount

of the backscatter available for interaction with the detector. Finally, this experiment used a 662

keV source, at lower source energy there may be greater amounts of backscattered photons

generated by the scattering medium since the photon – material interaction increases with

decreasing energy as predicted by the Klein-Nishina formula for the differential cross section [4].

Next, we move to the development of parametric equations to describe detector response.

5.4   Developing Parametric Equation

The integrated, individual scattering contributions as a function of Source-Detector unit

distance from the wall, as modeled in MCNP, are presented in Figures 19 – 21. They represent

the net count of backscattered photons from the scattering wall in three different configurations

of steel and concrete scattering mediums evaluated over source photon energies from 200 keV to

1200 keV.

The x axis is the source – detector unit distance from the wall and the y axis is the normalized

detector response.

Figure 20: MATLAB generated fit curves comparing simulated detector responses as a function of distance for steel and concrete scattering medium (for the Lateral Wall configuration dataset). Each data point represents the integrated detector response and each curve represents the detector response for the source photon energies from 200 keV to 1200 keV (evaluated over the 70 keV – 350 keV energy window).
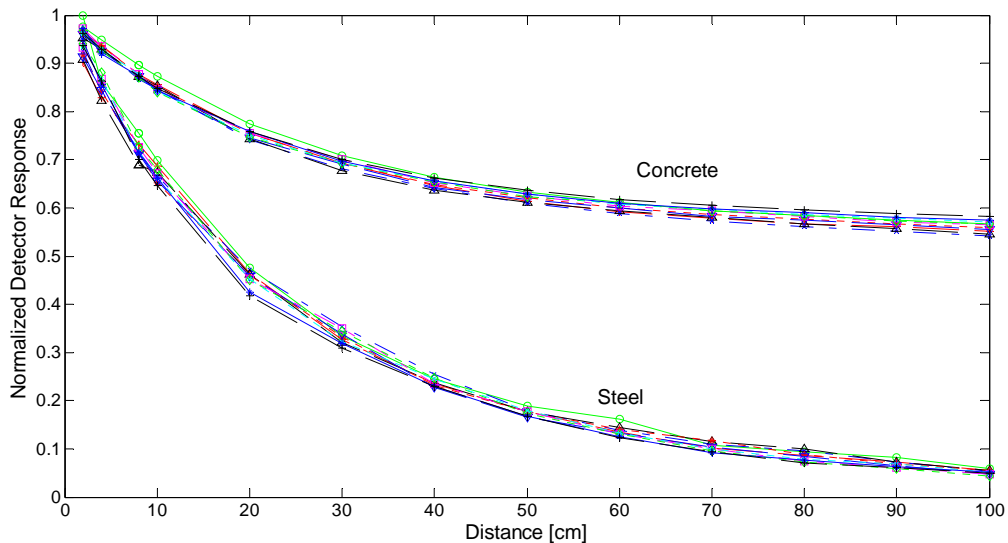
Figure 21 MATLAB generated fit curves comparing simulated detector responses as function of distance for steel and concrete scattering medium (for the Wall - Source - Detector configuration dataset). Each data point represents the integrated detector response and each curve represents the detector response for the source photon energies from 200 keV to 1200 keV (evaluated over the 70 keV – 350 keV energy window)
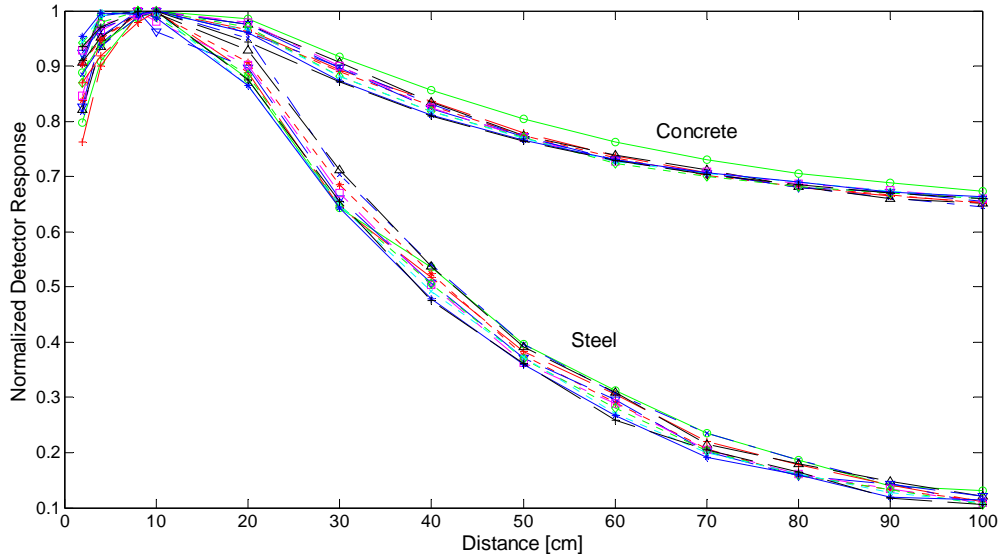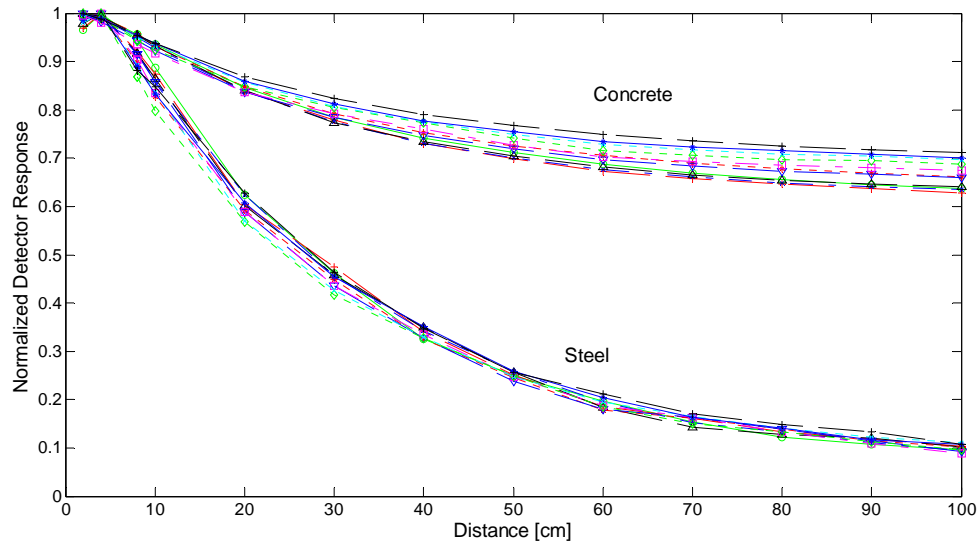
Figure 22 MATLAB generated fit curves comparing simulated detector responses as function of distance for steel and concrete scattering medium (for the Source - Wall - Detector configuration dataset). Each data point represents the integrated detector response and each curve represents the detector response for the source photon energies from 200 keV to 1200 keV (evaluated over the 70 keV – 350 keV energy window)

After trying several fit options the two term exponential algorithm fit the data better than any other algorithm. The fit equations are in the form:

$$f(x) = a*exp(b*x) + c*exp(d*x) \tag{5.1}$$

where a, b, c and d are coefficients calculated by the MATLAB fit algorithm and x is the distance from the wall. The lateral model curve fit used two separate fittings; the first for the four data points and the second for the last 10 data points. The algorithms could not fit the data using all 14 data points and provided an R^2=0.86 at 600 keV. Since R^2 is the statistical measure of how well a regression line approximates the real real data points on a scale with values from 0 to 1, values closer to 1 are more likely to predict the real data points. Using only the last 10 points changed the R^2 to greater than 0.98 for that configuartion. Using the two fit equations for

the Lateral Wall configuration does not a present a problem for this study because all lateral

surfaces are at least 75 cm from the detector and the fit equation nicely predicts the behavior of

the data points beyond 20 cm. As expected, the amount of backscatter is significantly less for

steel than for concrete. Steel is much denser than concrete and it has a higher crosssection for

photon absorption so it absorbs many more photons than concrete. In general the curve fit R^2

values are greater than 0.98 for all data fits and the fit equations with numerical value for a, b, c

and d are presented in appendix F of this document.

The error for the calculations was determined by propagating the relative error generated

from the MCNP simulation using the quadrature sum formula:

$$\sigma_u = \sqrt{\sigma_x^2 + \sigma_y^2} + ... \qquad\qquad (5.2)$$

where x and y are the measured number of counts, u = x+y or u=x-y and σ_x and σ_y are the errors

associated with the measured number of counts. The error was propagated twice, first by

subtracting the source photon and background contribution and then by integrating the individual

energy depositions in each of the the energy bins, for each configuration. The overall relative

error after propagation is approximately 0.0042 counts at 200 keV at 0 cm to approximately

0.0058 counts for 1200 keV at 100 cm distance (for all configurations). Next, the integrated

dataset was plotted as a function of source photon energy. The following series of figures show

the same normalized detector response as a function of source photons energies. The purpose of

these plots was to determine the detector response behavior as a function of source photon

energies and to determine the presence of a trend in the detector response as source photon

energies change.

47
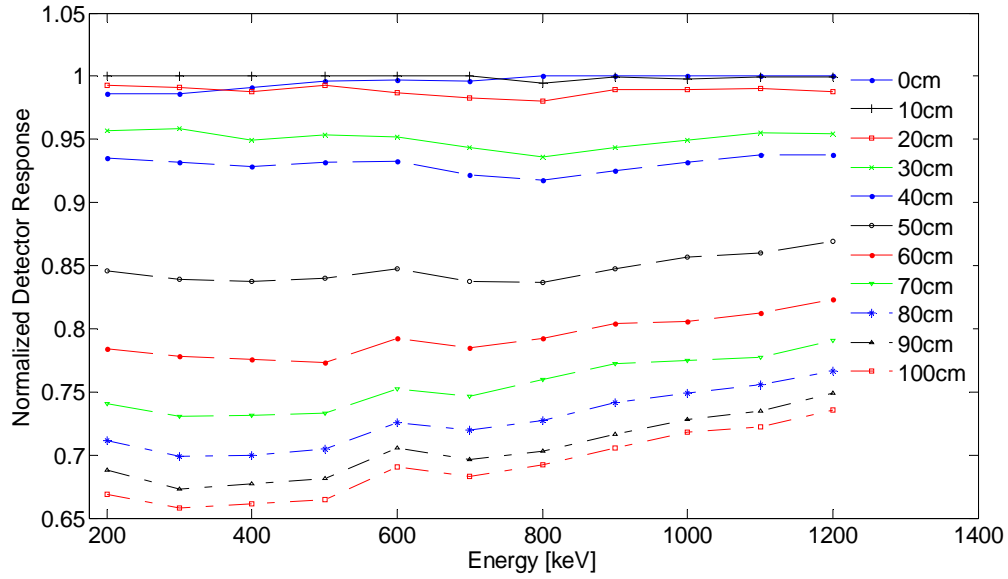
Figure 23: Detector response as a function of source photon energy for the Source – Detector – Wall configuration
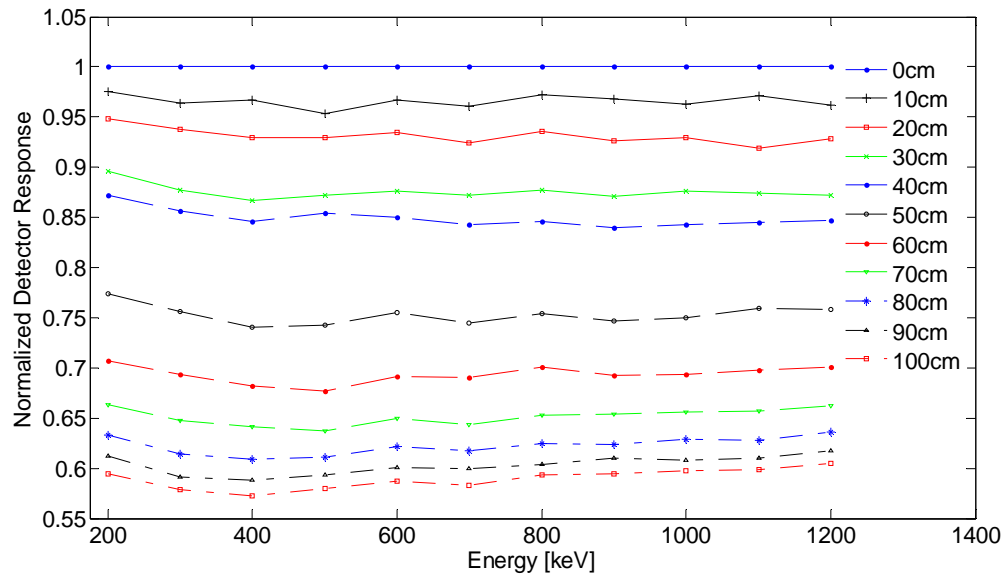
Figure 24: Detector response as a function of source photon energy for the Wall – Source – Detector configuration.
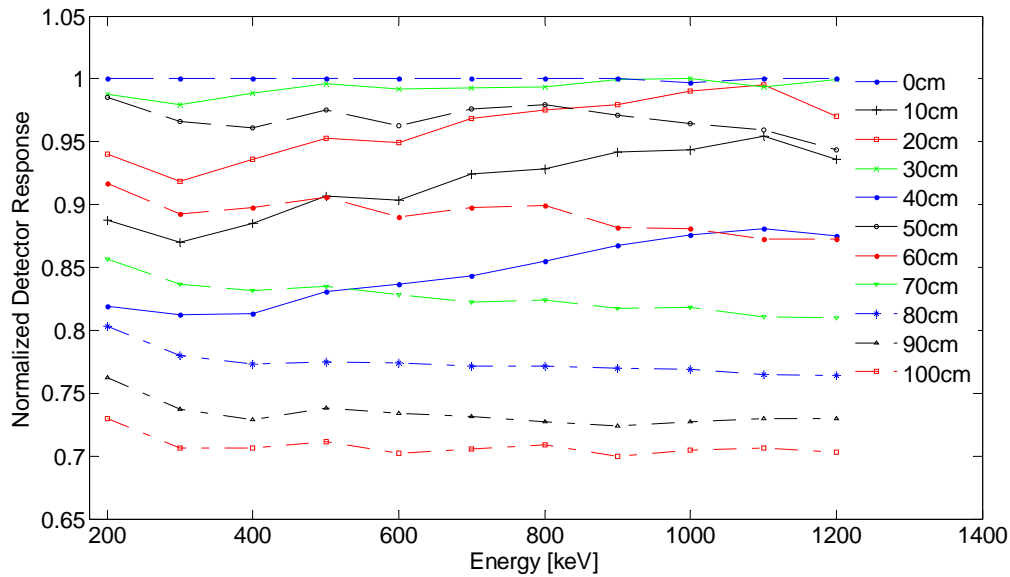
Figure 25: Detector response as a function of source photon energy for the Lateral Wall configuration.

For the S-D-W configuration (figure 22) the response are generally flat or decrease slightly for detector distances from 0 cm to 30 cm but beyond 40 cm as the source photon energy increases, the detector responses also increases. The change in the detector response also becomes greater as the distances from the wall increase. As an example, in the 100 cm S-D-W configuration plot, the detector response increases at a higher rate from 700 keV to 1200 keV than it does from 300keV to 500keV. A similar trend was observed in the Wall – Source – Detector (W-S-D) configuration but was only apparent at greater distances. A possible explanation for this behavior is that at farther distances, the higher energy photons have a slightly higher probability to scatter more than once and still have a chance for interacting with the detector than at the lower energies. At the lower source energies, especially at smaller distances, the photons are probably absorbed in the detector within scattering one time or else leave the system entirely. This would explain why the responses are flatter or slightly decrease at lower

source energies and increase at higher source energies. The Lateral Wall configuration response behaved differently than the first two configurations; it displayed a combination of flat and increasing detector responses throughout the distances. The Lateral Wall configuration is different than the other two because in this configuration the wall spans across both the source and detector. It is likely that the wall is generating many more backscattered photons at closer distances to the source that are registering in the detector. This interaction is also the likely reason for the "knee" seen in the lateral wall configuration detector response as a function of distance (figure 19).

Next, a test prediction response was generated using the fit equations derived from the data presented in figures 19 – 21. Responses were calculated for a test configuration where a detector was placed adjacent to a lateral wall and moved away from the front wall in 10 cm increments (in a manner similar to the results presented in the preceding sections). Next, the distance from the lateral wall increased by 20 cm and the detector moved again, from 0 cm to 100 cm from the front wall. The test was repeated for 40 cm and 80 cm lateral distance and the results plotted (figure 26) The purpose of this test was to assess the behavior of the response curves as a function of distance from the front wall and as a function of distance from the lateral wall; that is, to determine if the difference between the responses were apparent at distances closer to the walls versus at distances farther from the walls.
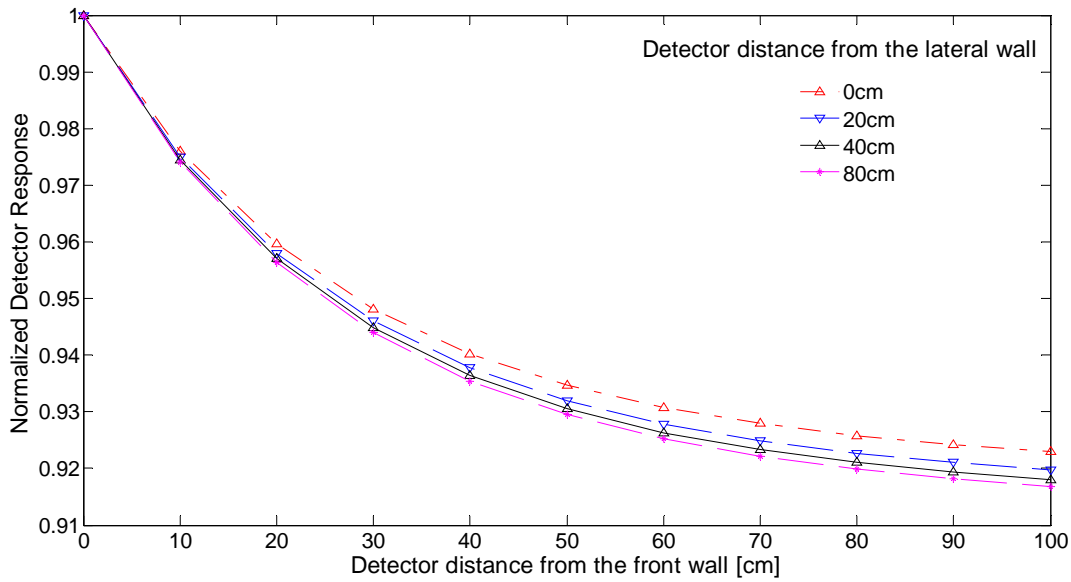
Figure 26: Calculated, normalized detector response at four detector distances from the lateral wall scattering medium. Though responses are individually identifiable, the responses are statistically indistinguishable.

The normalized detector responses plotted as a function of distance show that though the responses are similar, the changes in the detector response were apparent. However, the error bars overlap for all the responses and make them statistically indistinguishable from one another. Though this may seem like a problem at first, one must remember that the error bars are a function of the counts in each energy bin. By raising the number of simulated particles in the models, the number of counts in each bin can also be raised, thereby lowering the error. Therefore, the behavior of the error bars does not automatically negate the fact the responses are distinct and show the difference in detector response at varying distance. Clearly, there is a difference in the calculated response at 0 cm versus the calculated response at 80 cm. Next, the normalized calculated response at 700 keV is compared to the 662keV observed response that shows that the calculated results are much more in agreement.

5.4.1 Comparison of Normalized Predicted Response at 700 keV to Observed Response at 662 keV

The calculated results from the individual scattering contributions are added from the six configurations, normalized and compared to the normalized observed detector response. The predicted results are compared at 700 keV because the individual scattering medium responses were modeled in 100 keV increments, as a result the predictions can only be calculated in 100 keV increments and 700 keV is closests to the available Cs-137 source with 662 keV photons. The results are presented in figure 26.
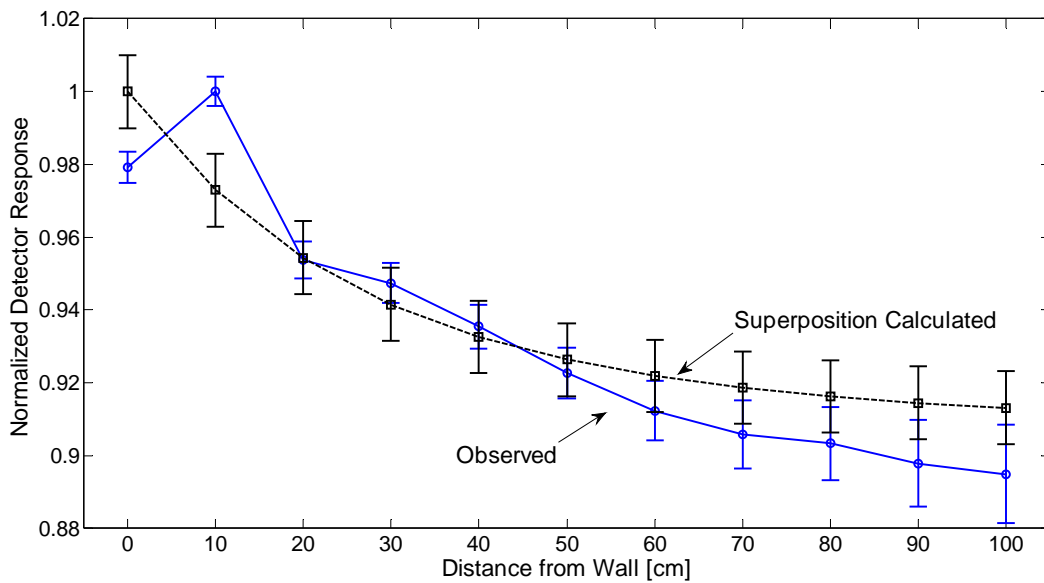
Figure 27: Comparison of predicted and observed detector response. The predicted response was calculated using the superposition principle. Normalized results from both methodologies are in good agreement.

The calculated response underestimates the observed response at four out of eleven data point but the data sets follow the same trend and all values are within 4% of each other. Observed error values are also similar to the initial experimental error calculations discussed in

the methodology section. The maximum relative error for the calculated method however is significantly lower at approximately 0.015 counts at 700 keV. Error in this methodology can not be quantified absolutely because the total error is based on the propagated error of the relative error from the individual energy bins from each of the configurations. The number of particles simulated in MCNP can raise or lower the error in the individual bins so the important information is the trend of the calculated response rather than the error values associated with them. Incidently, the acceptable level for an individual bin relative error for the pulse height tallies was set at 0.05 or less; the same values for the calculated predictions are very close at 0.07 over the energy window from 0 keV – 400 keV. This again reinforces that the high error for the predicted response is really due to the error propagation process and not the prediction methodology.

5.4.2 Predicted Response Using 3-Dimensional Scatter Contribution

In order to generalize the prediction methodology so that it can predict not only the response as a function of distance but also the response as a function of energy, the concrete medium responses are plotted versus distance and energy. MATLAB surface fit tool was used to fit the data and generate fit equations for the three configurations. In a method similar to the 2-dimension model, super positioning the individual contributions from these equations at the appropriate distance and energy can predict the overall detector response at a given distance and energy. The surface plots and the resulting fit equations are presented in figures 27 - 29.

Figure 28: A 3-D surface plot generated by plotting the detector response as a function of distance and energy. The resulting fit equation can be used to calculate the detector response for this configuration

$$f(x,y) = 1.019 - 0.008651 * x - 5.448e - 005 * y + 4.715e -$$

$$005 * x^2 + 9.953e - 007 * x * y + p02 * y^2; R - square: 0.9911$$

(5.3)
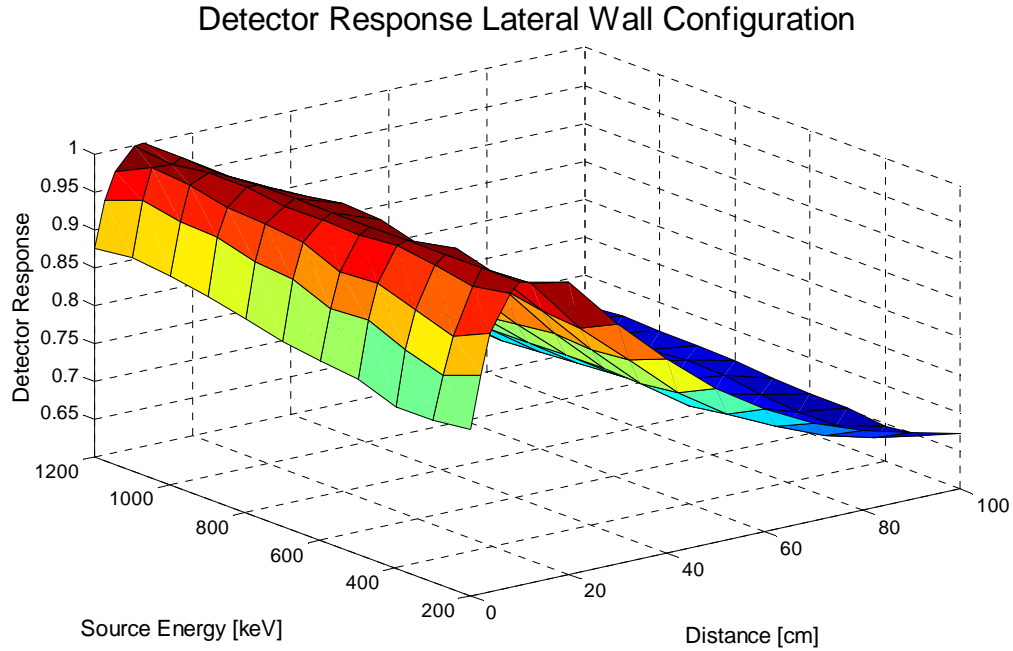
Figure 29: A 3-D surface plot generated by plotting the detector response as a function of distance and energy. The resulting fit equation can be used to calculate the detector response for this configuration

$$f(10cm - 100cm, y) = 1.125 - 0.008382 * x - 6.077e - 005 * y +$$

$$3.827e - 005 * x^2 + 2.585e - 007 * x * y + 2.23e - 008 * y^2; \quad R -$$

$$square: 0.989$$

$$f(0cm - 8cm, y) = 0.7813 + 0.04193 * x + 0.0001128 * y -$$

$$0.002133 * x^2 + -8.556e - 006 * x * y - 1.843e - 008 * y^2; \quad R -$$
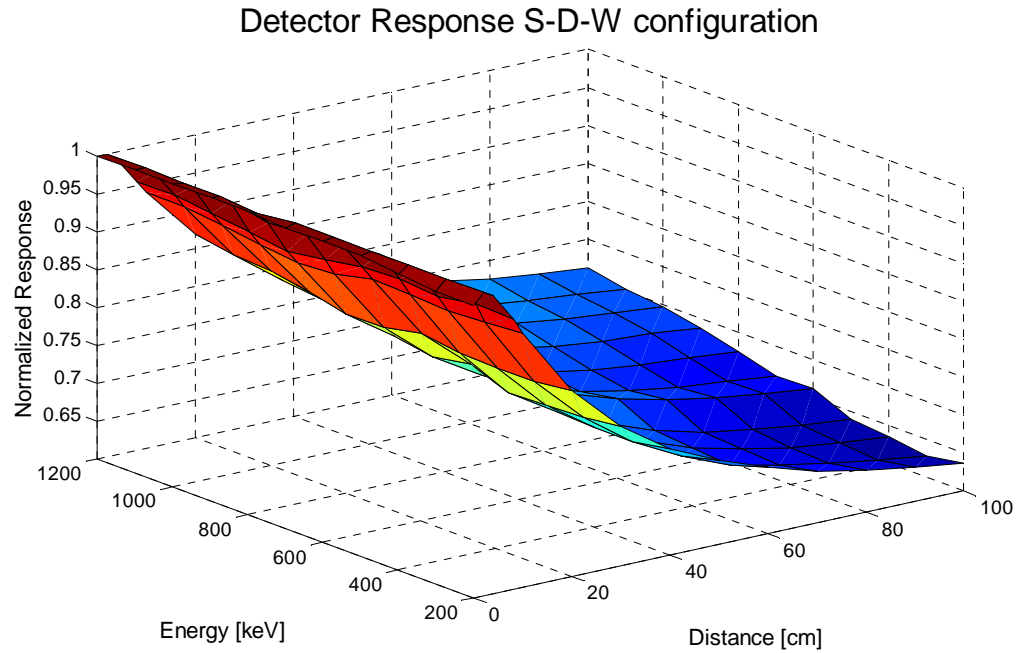
$$square: 0.9778$$

(5.4)
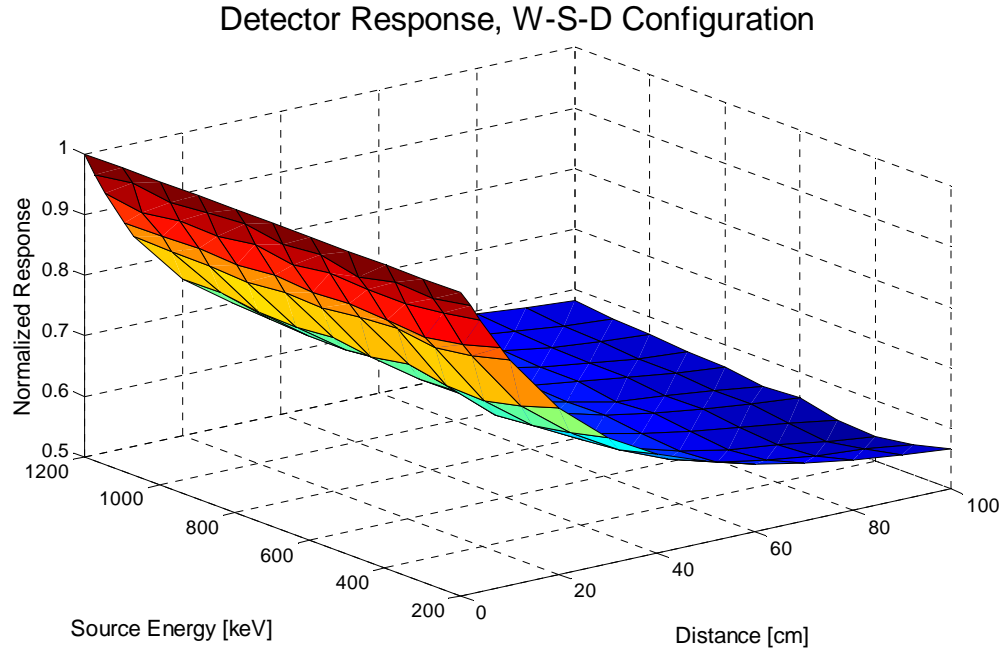
Figure 30: A 3-D surface plot generated by plotting the detector response as a function of distance and energy. The resulting fit equation can be used to calculate the detector response for this configuration

$$f(x,y) = 0.9909 - 0.01059 * x - 7.217e - 005 * y + 6.529e -$$

$$005 * x\hat{}2 + 4.119e - 007 * x * y + 4.466e - 008 * y\hat{}2 ; R - \qquad (5.5)$$

$$square: 0.981$$

MATLAB surface fitting tool offered limited fitting algorithms that could fit the data. It

was more desirable to use exponential and power fitting algorithms to fit the data but MATLAB

could not fit the three dimensional data very well using those algorithms. All configurations

were fitted using polynomial fits using two degrees of distance and energy. Similar to the

previous methodology, the Lateral Wall equation was fitted using two separate fitting.

Generally, all fit equation described the detector response well with an R^2 of 0.98. However, the

polynomial fitting presents a problem because polynomials fits are only correct over the

56

distances used to formulate it and cannot be used to extrapolate beyond the range of the observed data

Comparing the predicted responses using surface curve fits and the individual curve fit to the observed behavior shows that the normalized predictions are within 4% of the observed results (Figure 30).
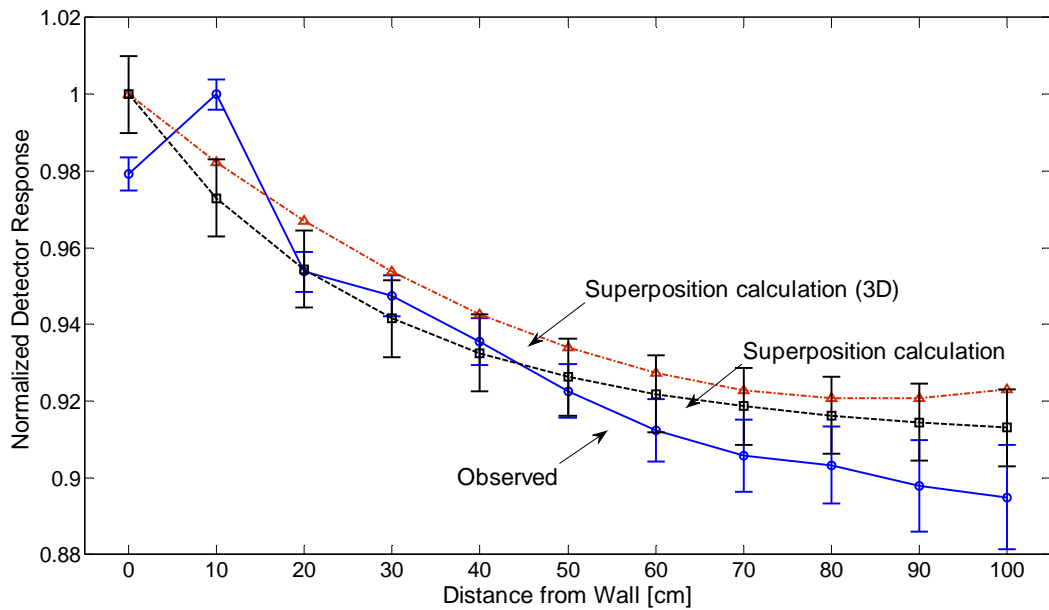
Figure 31: Comparison of observed and predicted responses from the superposition of individual responses and from the superposition of the responses calculated using the 3 dimensional surface plots fit equations. All responses are in general agreement from 0 cm – 90 cm.

A noteworthy feature in the surface fit calculations is the increased response of the surface fit prediction from 90 cm to 100 cm. The feature indicates an increasing detector response with increasing distance. This should not be possible and is probably due to the polynomial fitting algorithm used to calculate the response; therefore in this case the predictions are only valid from 0 cm to 90 cm (figure 30).

Though the normalized results are not in perfect agreement, they very similar over all distances. As more modeling and experimentation is conducted, this methodology can be refined to provide results more in agreement with the observed values. As an initial conclusion results from both methods slightly overestimate the observed detector response beyond 50 cm distance but are in agreement with the general behavior of the observed response.

VI.   Conclusions and Recommendations for future study

The purpose of this research was to demonstrate three things: First, a methodology to predict detector response without using lengthy MCNP models. Second, show that radionuclide identification is possible without using peak photons and finally, deducing a detector employment/emplacement strategy for maximizing backscatters photon count. The particle current simulations show photons backscatter peaks generated from the 200 keV – 1200 keV source photons register in the tally surfaces at energies that are captured in an energy window spanning from 70 keV – 370 keV.   This energy region captures the changes in the backscatter that is dependent on source photon energy and material composition. Because backscatter photon behavior varies with source photon energy, libraries of backscatter spectrum generated from the photon – material interaction can be catalogued and used for material identification. The results from parametric equations based on the relationship between scattering medium, source location, and detector placement show that a parametric equation can predict detector response. Finally, all modeled and experimental results suggest that to maximize the contribution from the backscattered photons, the detectors should be employed within 10 cm of a scattering medium.

By far the most important discovery out of the three findings is that parametric equations can predict detector response and the methodology is significantly faster at predicting background contribution and detector response. Since faster predictions are important in achieving faster detection methodologies, the parametric equations promise to speed up the process significantly.   This research also focused on lower energy backscattered gammas for improving detection rather than the traditional focus on peak photons. Though backscattering

has been studied in other research, characterizing the behavior of the backscattered photons as a function of distance and different materials is novel. To achieve this, the particle current simulations showed that characterization using backscattering is possible and may result in another way to identify radio-nuclides. These methodologies need to become part of a larger strategy where faster models predict response from radiation sources and where materials are identified using other signatures as well. This research serves as a first step in that direction. The results from the research were divided into the MCNP tallies and the parameterization of the detector response. The conclusions from those two areas are discussed next.

6.1   MCNP Tallies

MCNP tallies are an essential tool in developing an intuition of the detector response due to scattering from a scattering medium. The surface current tally (F1 tally) does this by providing the result of the photon current in the positive and the negative direction from the normal to the tally surface. However, a limitation of this tally function was discovered in the research. When asked to perform an F1 tally, the software tallied the particle current across the span of the whole simulation geometry and not in any particular feature of the simulation. For example, when asked to provide backscatter on one surface of a detector volume, it was unable to distinguish the backscattering contribution into one surface of the detector volume from the backscattering through the same surface as if it were spanning across the whole simulation geometry. Despite its limitation, it was a great tool for exploring the differences in the amount of backscatter while varying variables like materials, thickness and geometry using simple simulation geometry and lower particle counts. The tally however, was unable to generate data to establish the relationship between the detector response and the scattering medium surface area. The follow on research needs to investigate the response behavior as a function of solid

angles and detector distance from the scattering medium. Over all, F1 offered a quick method to predict general behavior of a scattering experiment without running lengthier pulse height tallies.

Pulse height tally function (F8 tally) on the other hand was better at predicting behavior within specific tally cells but in order to produce results with low errors it had to simulate significantly more particles to produce results with low relative errors. Therefore, it took significantly more time to run than the simpler surface current tally.

F8 tally showed similar results to the F1 tally results. Both tallies established a distance from 0 cm – 20 cm where photon backscatter was more available for interaction. The data generated by the F8 tally clearly showed the relationship between the distance of the detector from the scattering medium and the backscattered photons in the detector. Also the comparison of F8 tallies for concrete and steel showed that the type of material affect the amount of the benefit from the backscatter. Denser materials not only absorb more photons but generate maximum backscatter with smaller amounts of materials. Future study needs to explore common building materials like wood, aluminum, sheetrock, and glass to explore the effects on the Compton continuum using different materials and source energies. The study also needs to generalize common structural features and their shapes into equivalent simplified geometries. For example, can a tree be modeled as a cylindrical column of water? Developing these generalities will translate into detector responses based on simple geometrical shapes that can be parameterized into equations able to predict detector responses.

6.2 Parameterization of detector responses

An obvious advantage of parametric methods is faster calculations time than MCNP modeling. Where the MCNP took approximately 80 minutes to calculate, the parametric

equations can predict in seconds. However, before we can confidently predict detector responses using them, the fitting algorithms must fit the data points completely and predict the detector behavior across greater distances and source energy values. Polynomial fitting algorithms must be replaced by other algorithms able to go beyond the distances used to formulate the fits. Also an inherent problem with the methodologies is the larger error due to error propagation in the calculations. A way to reconcile the error with the correct response must be understood before the predicted results can be trusted. A reaslistic detector response can only be predicted once these methodologies have been refined. The 3- dimensional plotting and fitting could be improved by trying various fitting algorithms for models with incrementaly increasing source energies and must be explored in any future study. Overall the predictions based on parametric equations promise a comparable detector response prediction once they are refined.

6.3   Closing

The project under which this research was conducted aims to identify radioactive sources using a combination of Polarimetric-Hyperspectral imagery (PHSI) and traditional radio-nuclide identification. PHSI can provide material information that can be fed to parametric equations to calculate the expected detector response from background and a source in a detection scenario. The advantage of this methodology is the speed with which it can predict the response but the limitation is that it only works in the Compton continuum of the detector spectrum. Unfortunately, libraries containing the predicted detector behaviors in the Compton continuum for various energies and materials do not exist yet. They must be developed in conjunction with the predictive equations. Once both of these are developed, the combined PHSI – parametric prediction system will offer a method that will be much faster at predicting detector responses than the current models.

VII. Appendices

Appendix A

Input file for a F1 tally in simulation geometry. Material type, thickness and source energy can be manipulated to generate a variety of results.

```
MCNPX Visual Editor Version X_24E
c     10x larger model to evaluate backscatter
    1    204 -0.001225 -1 2 3 4 5 6 7 8 9   $The universe
    2    228   -2.35 -2   $conc wall
    3    204 -0.001225 -3   $0cm
    4    204 -0.001225 -4   $10cm
    5    204 -0.001225 -5   $20cm
    6    204 -0.001225 -6   $30cm
    7    204 -0.001225 -7   $40cm
    8    204 -0.001225 -8   $50cm
    9    204 -0.001225 -9   $60cm
   10     0         1   $outside

    1        rpp 0 15 0 180 0 45   $The universe
    2        rpp 0 15 0 20 0 45   $conc wall
    3        rpp 1 14.9 20.1 26 0.1 449
    4        rpp 1 14.9 30 36 0.1 44.9   $10cm
    5        rpp 1 14.9 40 46 0.1 44.9   $20cm
    6        rpp 1 14.9 50 56 0.1 44.9   $30cm
    7        rpp 1 14.9 60 66 0.1 44.9   $40cm
    8        rpp 1 14.9 70 76 0.1 44.9   $50cm
    9        rpp 1 14.9 80 86 0.1 44.9   $60cm

mode   p
m204  7000.02p       -0.755636   $air (US S. Atm at sea level)
      8000.02p       -0.231475 18000.02p      -0.012889
m228  1000.02p       -0.005558   $concrete (ordinary with ENDF-VI)
      8000.02p      -0.4980765 11000.02p      -0.017101 12000.02p     -
0.002565
      13000.02p      -0.045746 14000.02p      -0.3150923 16000.02p     -
0.001283
      19000.02p      -0.019239 20000.02p      -0.0829411 26000.02p     -
0.012398
imp:p   1 8r         0                $ 1, 10
sdef pos = 7.5 100 22.5 erg=.600
nps 10000000
c Tally
f1:p 3.4 4.4 5.4 6.4 7.4 8.4 9.4
c1 -1 0 1
```

Appendix B

A sample Input file for a F8 tally in simulation geometry in the Wall-Source-Detector configuration.

```
MCNPX Visual Editor Version X_24E
c     Created on: Monday, November 12, 2012 at 10:29
c WSD
    1   204 -0.001225 -1 2 3   $The exp area
    2   228   -2.35 -2   $Conc wall
    3   100   -3.87 -3   $NaI detector Constant
    4    0        1   $Outside

c    Begins the surfaces
    1        rpp 0 300 19.99 150 0 300   $The universe
    2        rpp 0 300 130 150 0 300   $The concrete wall
    3        rcc 150 20 75 0 8 0 4   $The 3x3 NaI detector

mode  p
m204  7014.70c      -0.755636  $air (US S. Atm at sea level)
      8016.70c      -0.231475 18036.70c     -3.9e-005 18038.70c
-8e-006
      18040.70c     -0.012842
m228  1001.70c      -0.005558  $concrete (ordinary with ENDF-VI)
      8016.70c      -0.498076 11023.70c     -0.017101 12024.70c     -
0.001999
      12025.70c     -0.000264 12026.70c     -0.000302 13027.70c     -
0.045746
      14028.70c     -0.289486 14029.70c     -0.015181 14030.70c     -
0.010425
      16032.70c     -0.001216 16033.70c      -1e-005 16034.70c     -
5.7e-005
      19039.70c     -0.01788 19040.70c      -2e-006 19041.70c     -
0.001357
      20040.70c     -0.08019 20042.70c     -0.000562 20043.70c      -
0.00012
      20044.70c     -0.00188 20046.70c      -4e-006 20048.70c     -
0.000186
      26054.70c     -0.000707 26056.70c      -0.01139 26057.70c     -
0.000265
      26058.70c     -3.6e-005
m100  81000.01p       0.001  $NaI(Tl)
      11000.01p       0.499 53000.01p        0.5
imp:p   1 2r       0            $ 1, 4
sdef pos=150 99.9 75 erg=.600
nps 100000000
c F8 tally
f8:p 3
   e8 .1e-15 .001 .01 59i 0.6
```

Appendix C

A sample Input file for a F8 tally in simulation geometry in the Source- Wall-Detector configuration.

```
MCNPX Visual Editor Version X_24E
c     Created on: Monday, November 12, 2012 at 10:29
c source det wall
    1    204 -0.001225 -1 2 3   $The exp area
    2    228   -2.35 -2   $Conc wall
    3    100   -3.87 -3   $NaI detector Constant
    4     0            1   $Outside

c    Begins the surfaces
    1       rpp 0 300 0 200 0 300   $The universe
    2       rpp 0 300 0 19.99 0 300   $The concrete wall
    3       rcc 150 20 75 0 8 0 4   $The 3x3 NaI detector

mode  p
m204  7014.70c       -0.755636  $air (US S. Atm at sea level)
      8016.70c       -0.231475 18036.70c      -3.9e-005 18038.70c
-8e-006
      18040.70c      -0.012842
m228  1001.70c       -0.005558  $concrete (ordinary with ENDF-VI)
      8016.70c       -0.498076 11023.70c      -0.017101 12024.70c    -
0.001999
      12025.70c      -0.000264 12026.70c      -0.000302 13027.70c    -
0.045746
      14028.70c      -0.289486 14029.70c      -0.015181 14030.70c    -
0.010425
      16032.70c      -0.001216 16033.70c       -1e-005 16034.70c    -
5.7e-005
      19039.70c      -0.01788 19040.70c       -2e-006 19041.70c    -
0.001357
      20040.70c      -0.08019 20042.70c      -0.000562 20043.70c     -
0.00012
      20044.70c      -0.00188 20046.70c       -4e-006 20048.70c    -
0.000186
      26054.70c      -0.000707 26056.70c      -0.01139 26057.70c    -
0.000265
      26058.70c      -3.6e-005
m100  81000.01p        0.001  $NaI(Tl)
      11000.01p        0.499 53000.01p          0.5
imp:p   1 2r          0                $ 1, 4
sdef pos=150 99.9 75 erg=.600
nps 100000000
c F8 tally
f8:p 3
  e8 .1e-15 .001 .01 59i 0.6
```

A sample Input file for a F8 tally in simulation geometry in the Lateral wall configuration.

```
MCNPX Visual Editor Version X_24E
c     Created on: Monday, November 12, 2012 at 10:29
c Perp Wall
    1   204 -0.001225 -1 2 3   $The exp area
    2   228   -2.35 -2   $Conc wall
    3   100   -3.87 -3   $NaI detector Constant
    4    0         1   $Outside

c    Begins the surfaces
    1       rpp 0 300 0 300 0 159   $The universe
    2       rpp 0 300 0 300 139 159 $The concrete wall
    3       rcc 150 20 74.9 0 8 0 4   $The 3x3 NaI detector

mode  p
m204  7014.70c      -0.755636  $air (US S. Atm at sea level)
      8016.70c      -0.231475 18036.70c      -3.9e-005 18038.70c
-8e-006
      18040.70c     -0.012842
m228  1001.70c      -0.005558  $concrete (ordinary with ENDF-VI)
      8016.70c      -0.498076 11023.70c      -0.017101 12024.70c     -
0.001999
      12025.70c     -0.000264 12026.70c      -0.000302 13027.70c     -
0.045746
      14028.70c     -0.289486 14029.70c      -0.015181 14030.70c     -
0.010425
      16032.70c     -0.001216 16033.70c       -1e-005 16034.70c     -
5.7e-005
      19039.70c      -0.01788 19040.70c      -2e-006 19041.70c      -
0.001357
      20040.70c      -0.08019 20042.70c      -0.000562 20043.70c      -
0.00012
      20044.70c      -0.00188 20046.70c      -4e-006 20048.70c      -
0.000186
      26054.70c     -0.000707 26056.70c      -0.01139 26057.70c      -
0.000265
      26058.70c     -3.6e-005
m100  81000.01p        0.001  $NaI(Tl)
      11000.01p        0.499 53000.01p         0.5
imp:p   1 2r        0             $ 1, 4
sdef pos=150 100 74.9 erg=.600
nps 100000000
c F8 tally
f8:p 3
e8 .1e-15 .001 .01 59i 0.6
```

Appendix E

Equipment listing and Energy Calibration

Equipment	SN	Setting
Plastic Detector Model DA1230PP	313818	NA
Preamp	6606	0pF
Bias (Ortec 478)	41975	1000 Volts
Amplifier (Ortec 578)	4745	CG: 100
NaI 3x3	4-00024-I	
Preamp	6508	100pF
Ortec DART	23825	800 Volts
		6μsec
		CG: 44

Energy Calibration

Energy calibration for the NaI(Tl) detector is conducted so that the channels can be assigned an energy bin value for photon deposition. The calibration was conducted using the Cs137, and the Co60 source. The energy calibration equation was determined to be E = 3.8907x - 29.514, R^2 = 0.9999. No energy calibration for the PVT detector is required since gross counts are compared over an energy window.

Apendix F   Concrete Fit equations Lateral wall configuration (points 1 – 5)

f200a(x) = 1.168*exp(-0.007907*x)-0.3487*exp(-0.1477 *x)
f300a(x) = 1.123*exp(-0.00227*x) -0.3105*exp(-0.1157*x)
f400a(x) = 1.138*exp(-0.006231*x)-0.3245*exp(-0.1554*x)
f500a(x) = 1.155*exp(-0.008799*x)-0.3235*exp(-0.1737*x)
f600a(x) = 1.148*exp(-0.007647*x)-0.3115 *exp(-0.159*x)
f700a(x) = 1.012*exp(-0.0008106*x)-0.1695*exp(-0.344*x)
f800a(x) = 1.038*exp(-0.003071*x)-0.1843*exp(-0.3031*x)
f900a(x) = 1.038*exp(-0.003058*x)-0.1703*exp(-0.3261*x)
f1000a(x) = -0.3205*exp(-0.2009*x)+1.195*exp(-0.0141*x)
f1100a(x) = 1.033 *exp(-0.003342*x)-0.1525*exp(-0.4031*x)
f1200a(x) = 1.089*exp(-0.005943*x) -0.2145*exp(-0.2095*x)

Concrete Fit equations Lateral wall configuration (points 5 – 14)

f200(x)=1.08*exp(-0.005855*x)+0.0003852*exp(0.05277*x)
f300(x)=1.08*exp(-0.006658*x)+0.001619*exp(0.04128*x)
f400(x)=1.08*exp(-0.006966*x)+0.003698*exp(0.03403*x)
f500(x)=1.086*exp(-0.00665*x)+0.001163*exp(0.04413*x)
f600(x)=1.08*exp(-0.007135*x)+0.005225*exp(0.03191*x)
f700(x)=1.088*exp(-0.007413*x)+0.006484*exp(0.0309*x)
f800(x)=0.007132*exp(0.03046*x)+1.09*exp(-0.007489*x)
f900(x)=1.083*exp(-0.007938*x)+0.01191*exp(0.0269*x)
f1000(x)=1.068*exp(-0.008167*x)+0.02225*exp(0.02171*x)
f1100(x)=1.02*exp(-0.009835*x)+0.07653*exp(0.01315*x)
f1200(x)=1.003*exp(-0.009989*x)+0.08751*exp(0.01207*x)

Concrete Fit equations WSD configurations

f200(x)=0.4081*exp(-0.04362*x)+0.6142*exp(-0.0009082*x)
f300(x)=0.4297*exp(-0.04028*x)+0.571*exp(-0.0004724*x)
f400(x)=0.3835*exp(-0.05095*x)+0.6239*exp(-0.001468*x)
f500(x)=0.41*exp(-0.06194*x)+0.6445*exp(-0.001659*x)
f600(x)=0.3943*exp(-0.04428*x)+0.602*exp(-0.0008108*x)
f700(x)=0.3784*exp(-0.04759*x)+0.614*exp(-0.001038*x)
f900(x)=0.3482*exp(-0.05002*x)+0.6361*exp(-0.001218*x)
f1000(x)=0.365*exp(-0.04693*x)+0.6195*exp(-0.0008708*x)
f1100(x)=0.3936*exp(-0.03955*x)+0.5816*exp(-0.0002259*x)
f1200(x)=0.3684*exp(-0.04428*x)+0.6141*exp(-0.0006063*x)

Concrete Fit equations SDW configurations

f200(x) = 0.3717*exp(-0.04059*x) + 0.6944 *exp(-0.0009824*x)
f300(x) = 0.4214*exp(-0.03586*x) + 0.6393*exp(-0.0003525*x)
f400(x) = 0.4202*exp(-0.03575*x) + 0.6353 *exp(-0.0001944*x)
f500(x) = 0.4049*exp(-0.04004*x) + 0.6635*exp(-0.000482*x)
f600(x) = 0.3445*exp(-0.04253*x) + 0.7131*exp(-0.0008285*x)
f700(x) = 0.3617*exp(-0.03836*x) + 0.6771 *exp(-0.0003732*x)
f800(x) = 0.3734*exp(-0.03179*x) + 0.642*exp(0.0002582*x)
f900(x) = 0.3866*exp(-0.02847*x) + 0.6278*exp(0.0005903*x)
f1000(x) = 0.3306*exp(-0.038*x) + 0.707 *exp(-0.0002459*x)
f1100(x) = 0.3174*exp(-0.0417*x) + 0.7312 *exp(-0.0004836*x)
f1200(x) = 0.2889*exp(-0.03927*x) + 0.7469*exp(-0.0005726*x)

Steel Fit equations Lateral wall configuration

f200(x) = 1.441*exp(-0.02557*x) -7.145e+005*exp(-1.564 *x)
f300(x) = 1.497*exp(-0.02686*x) -2.341e+007*exp(-1.89*x)
f400(x) = 1.642*exp(-0.0278*x) -2.032e+006*exp(-1.594*x)
f500(x) = 1.622*exp(-0.02772*x) -18.43 *exp(-0.437*x)
f600(x) = 1.611*exp(-0.02853*x) -17.25 *exp(-0.4384*x)
f700(x) = 1.554*exp(-0.02805*x) -7.548e+006*exp(-1.739*x)
f800(x) = 1.59*exp(-0.0287*x) -6.685e+005*exp(-1.496*x)
f900(x) = 1.54*exp(-0.02822*x) -5.906e+005*exp(-1.505*x)
f1000(x) = 1.513*exp(-0.02813 *x) -1.575e+005*exp(-1.39*x)
f1100(x) = 1.528*exp(-0.02874*x) -9.008e+005*exp(-1.555*x)
f1200(x) = -2.278e+006*exp(-1.646*x) + 1.554*exp(-0.02901*x)

Steel Fit equations WSD configuration

f200(x) = 0.6399*exp(-0.06585*x) + 0.4498 *exp(-0.01987*x)
f300(x) = 0.7583*exp(-0.05272*x) + 0.2826 *exp(-0.01685 *x)
f400(x) = 0.8758*exp(-0.03624 *x) + 0.05866*exp(-0.005236*x)
f500(x) = 0.6611*exp(-0.06147*x) + 0.3819*exp(-0.01853*x)
f600(x) = 0.7013*exp(-0.04691*x) + 0.2516 *exp(-0.01589 *x)
f700(x) = 0.852*exp(-0.04031*x) + 0.09526 *exp(-0.00938*x)
f800(x) = 0.3211 *exp(-0.07933*x) + 0.6912*exp(-0.02767*x)
f900(x) = 1.459e+006*exp(-1.695*x) + 0.8362*exp(-0.03054*x)
f1000(x) = 0.4845 *exp(-0.063*x) + 0.5081 *exp(-0.02341*x)
f1100(x) = 0.5779*exp(-0.1447*x) + 0.6953*exp(-0.02789*x)
f1200(x) = 0.7223*exp(-0.187*x) + 0.7122*exp(-0.02857*x)

Steel Fit equations SDW configuration

f200(x) = 1.185*exp(-0.03804*x) + 0.07712*exp(-0.001268*x)
f300(x) = 1.182*exp(-0.0346*x) + 0.02799*exp(0.009021*x)
f400(x) = 1.156*exp(-0.03396*x) +0.03489*exp(0.004955*x)
f500(x) = 1.174*exp(-0.033*x) + 0.01073*exp(0.01731*x)
f600(x) = 1.118*exp(-0.03456*x) + 0.0334*exp(0.007355*x)
f700(x) = 1.012*exp(-0.04646*x) + 0.2424*exp(-0.01022*x)
f800(x) = 0.8375*exp(-0.04748*x) + 0.3614*exp(-0.01473 *x)
f900(x) = 0.9286*exp(-0.04125*x) + 0.1989*exp(-0.00907*x)
f1000(x) = 0.9174*exp(-0.05165*x) + 0.3203*exp(-0.01155*x)
f1100(x) = 1.106*exp(-0.03217*x) + 0.02725 *exp(0.0084*x)
f1200(x) = 1.125*exp(-0.03377*x) + 0.04555*exp(0.005067*x)

Appendix G

Mean Free Path of photons in Concrete, Air and Steel

Energy [keV]	MFP, Concrete [cm]	MFP, Air [cm]	MFP, Steel [cm]
200	0.15	6488.2	0.878
600	5.2	9931.7	1.66
1250	7.3	14067.2	2.4

Works Cited

[1] International Atomic Energy Agency, "Technical Report Series 419," International Atomic Energy Agency, December 2003. [Online]. Available: http://www.world-nuclear.org/info/inf30.html. [Accessed 24 November 2010].

[2] S. M. T. Hoang, Y. Sangho and M. S. Gwang, "EXPERIMENTAL VALIDATION OF THE BACKSCATTERING GAMMA-RAY SPECTRA WITH THE MONTE CARLO CODE," *NUCLEAR ENGINEERING AND TECHNOLOGY,* vol. 43, no. 1, pp. 13 - 18, 2011.

[3] Rutgers Physics Department, "Laboratory Instructions, Physics 389," 02 2000. [Online]. Available: www.physics.rutgers.edu/ugrad/389/gamma.pdf. [Accessed 20 12 2012].

[4] G. F. Knoll, Radiation Detection and Measurement, Ann Arbor: Wiley, 2010.

[5] E. Siciliano, J. Ely, R. Kouzes, B. Milbrath and J. Schweppe, "Comparison of PVT and NaI(Tl) scintillators for vehicle portal monitor applications," *Nuclear Instruments and Methods in Physics Research,* vol. A, no. 550, pp. 647 - 674 , 2005.

[6] A. V. a. A. S. W. w. S. H. N. Oppenheim, Signals and Systems, New Jersey: Prentice Hall, 1997.

[7] E. M. H. Shuo-Sheng Tang, "Use of isotropic gamma sources for identifying anti-personnel landmines," *Applied Radiation and Isotopes,* vol. 61, pp. 3-10, 2004.

[8] University of California, Los Alamos National Laboratory, "MCNP — A General Monte Carlo N-Particle Transport Code, Version 5," Los Alamos National Laboratory, Los Alamos, 2003.

[9] Los Alamos National Lab, "MCNP — A General Monte Carlo N-Particle Transport Code, Version 5," in *Volume 1*, Berkley, Los Alamos National Lab, 2005.

[10] D. Reeder and S. P.C, "Performance of Large NaI(Tl) Gamma-Ray Detectors Over Temperature -50ºC to +60ºC," Pacific Northwest National Laboratory, Richland, 2004.

[11] Saint-Gobain Crystals, "Plastic Scintillators," Saint-Gobain, 20 12 2012. [Online]. Available: http://www.detectors.saint-gobain.com/Plastic-Scintillator.aspx. [Accessed 20 12 2012].

[12] A. R. E. Baker, "The Use of the Monte Carlo Technique in the Simulation of Small-Scale Dosimeters and Microdosimeters," University of Birmingham, Birmingham, 2011.

[13] J. H. Ely, R. T. Kouzes, B. D. Geelhood, J. E. Schweppe and R. A. Warner, "Discrimination of Naturally Occurring Radioactive Material in Plastic Scintillator Material," *IEEE TRANSACTIONS ON NUCLEAR*

SCIENCE, vol. 51, no. 4, pp. 172 - 1676, 2004.

[14] D. N. P. T. T. T. T. A. K. A. M. V. N. TRUONG THI HONG LOAN, "MONTE CARLO SIMULATION OF HPGe DETECTOR RESPONSE FUNCTION USING MCNP CODE," *Communications in Physics,* vol. 17, no. 1 , pp. 59 - 64, 2007.

[15] Dscraggs, "Klein-Nishina distribution," Wikipedia, 05 04 2009. [Online]. Available: http://en.wikipedia.org/wiki/File:Klein-Nishina_distribution.png. [Accessed 16 12 2012].

REPORT DOCUMENTATION PAGE

1. REPORT DATE (DD–MM–YYYY)	2. REPORT TYPE	3. DATES COVERED (From — To)
22-03-2013	Master's Thesis	October 2012 – March 2013

4. TITLE AND SUBTITLE	5a. CONTRACT NUMBER
Modeling Sodium Iodide Detector Response Using a Parametric Equations	5b. GRANT NUMBER
	5c. PROGRAM ELEMENT NUMBER

6. AUTHOR(S)	5d. PROJECT NUMBER
Sethi, Neeraj MAJ, U.S. Army	5e. TASK NUMBER
	5f. WORK UNIT NUMBER

7. PERFORMING ORGANIZATION NAME(S) AND ADDRESS(ES)	8. PERFORMING ORGANIZATION REPORT NUMBER
Air Force Institute of Technology Graduate School of Engineering and Management (AFIT/ENP) 2950 Hobson Way WPAFB OH 45433-7765	AFIT-ENP-13-M-30

9. SPONSORING / MONITORING AGENCY NAME(S) AND ADDRESS(ES)	10. SPONSOR/MONITOR'S ACRONYM(S)
Defense Threat Reduction Agency DTRA-RD-BA 8725 John J. Kingman Rd Ft. Belvoir, VA 22060 Attn: Col Jeffery Musk	DTRA
	11. SPONSOR/MONITOR'S REPORT NUMBER(S)

12. DISTRIBUTION / AVAILABILITY STATEMENT
APPROVED FOR PUBLIC RELEASE; DISTRIBUTION UNLIMITED

13. SUPPLEMENTARY NOTES   This material is declared a work of the U.S. Government and is not subject to copyright protection in the United States.

14. ABSTRACT
This research utilizes the relationship between source location, background radiation and detector placement to quantify an expected detector response from a 3x3 Sodium Iodide gamma detector. A parametric equation is developed to calculate the detector response as a function of distance and source photon energy. Using MCNP particle current and pulse height tally functions, backscattering photons are quantified as a function of material thickness and energy distribution. Three configurations of source – detector – scattering medium were modeled in MCNP using the pulse height tally functions, integrated over a 70keV – 360keV energy window and plotted as a function of the detector distance from the scattering medium. The resulting fit equations described the effects on detector response from the backscattered photons from any wall in a box shaped space. The superposition of the individual scattering contributions from six surfaces made up the total scattering contribution and predicted the overall expected detector response. The same data sets were also plotted and fitted as a function of distance and energy to produce 3 dimensional parametric equations that predicted detector response over ranges of distance and energy. The normalized superposition and 3D superposition calculated responses were within 4% of the observed responses.

15. SUBJECT TERMS
Parameterization of NaI detector response

16. SECURITY CLASSIFICATION OF:			17. LIMITATION OF ABSTRACT	18. NUMBER OF PAGES	19a. NAME OF RESPONSIBLE PERSON Major Benjamin R. Kowash, AFIT/ENP
a. REPORT	b. ABSTRACT	c. THIS PAGE	UU		19b. TELEPHONE NUMBER (Include Area Code) (937)255-3636, ext 4571
U	U	U		87	

Standard Form 298 (Rev. 8–98)
Prescribed by ANSI Std. Z39.18